A Macrocyclic Chelator that Selectively Binds Ln^{4+} over Ln^{3+} by a factor of 10^{29}

Tiffany A. Pham,[1,2] Alison B. Altman,[1,2] S. Chantal E. Stieber,[3,4] Corwin H. Booth,[2] Stosh A. Kozimor,[3] Wayne W. Lukens,[2] Daniel T. Olive,[2] Tolek Tyliszczak,[2] Jian Wang,[5] Stefan G. Minasian,[2]* and Kenneth N. Raymond[1,2]*

[1] University of California, Berkeley, California, 94720, United States
[2] Lawrence Berkeley National Laboratory, Berkeley, California, 94720, United States
[3] Los Alamos National Laboratory, Los Alamos, New Mexico, 87545, United States
[4] California State Polytechnic University, Pomona, CA 91768, United States
[5] Canadian Light Source, Saskatoon, Saskatchewan, S7N 2V3, Canada

Abstract. A tetravalent cerium macrocyclic complex (Ce**L**K_4) was prepared with an octadentate terephthalamide ligand comprised of hard catecholate donors, and characterized in the solution state by spectrophotometric titrations and electrochemistry, and in the crystal by X-ray diffraction. The solution state studies showed that **L** exhibits a remarkably high affinity towards Ce^{4+}, with log β_{110} = 61(2) and ΔG = -348 kJ/mol, compared with log β_{110} = 32.02(2) for the analogous Pr^{3+} complex. In addition, **L** exhibits an unusual preference for forming Ce$\mathbf{L}^{4-}$ relative to formation of the analogous actinide complex, Th$\mathbf{L}^{4-}$, which has β_{110} = 53.7(5). The extreme stabilization of tetravalent cerium relative to its trivalent state is also evidenced by the shift of 1.91 V in redox potential of the Ce^{3+}/Ce^{4+} couple of the complex (measured at -0.454 V vs. SHE). The unprecedented behavior prompted an electronic structure analysis using L_3 and $M_{5,4}$-edge X-ray absorption near-edge structure (XANES) spectroscopies and configuration interaction calculations, which showed that 4f orbital bonding in Ce**L**K_4 has partial covalent character owing to ligand-to-metal charge transfer (LMCT) in the ground state. The experimental results are presented in the context of earlier measurements on tetravalent cerium compounds, indicating that the amount LMCT for Ce**L**K_4 is similar to that observed for $[Et_4N]_2[CeCl_6]$ and CeO_2, and significantly less than that for the organometallic sandwich compound cerocene, $(C_8H_8)_2Ce$. A simple model to rationalize changes in 4f orbitals for tri- and tetravalent lanthanide and actinide compounds is also provided.

INTRODUCTION

Cerium is the only lanthanide element that is stable in the 4+ formal oxidation state in aqueous and organic solutions, molecular compounds, and extended solids.[1] This enhanced stability derives from the noble gas [Xe] configuration, which is reflected by cerium's low fourth ionization potential relative to the other lanthanides.[2] Accordingly, bonding with cerium has been regarded primarily as ionic. However, covalency is increasingly becoming an important component of bonding models used to describe tetravalent cerium by both chemists and physicists. The juxtaposition between these two models raises many important questions, such as whether the Ce 4f or the 5d orbitals are the drivers of covalent interactions in molecules, extended solids, metals and intermetallics. In addition, determining whether small amounts of covalency significantly impact physical properties or the outcome of chemical processes continues to be an experimental and computational challenge.

Much of the current understanding of cerium electronic structure comes from in-depth physical studies of extended solids and intermetallics. Cerium can be found in the +4 formal oxidation state in some non-molecular, extended solids such as Cs_2CeCl_6 and other binary halides,[3-6] CeO_2,[7] $Ce(SO_4)_2$,[8] and $[NH_4]_2[Ce(NO_3)_6]$,[9-10] among others.[11] These materials have been the subject of numerous synchrotron radiation based spectroscopy experiments, including X-ray photoelectron spectroscopy,[12] resonant inelastic X-ray scattering,[13] and X-ray absorption spectroscopies at the cerium L_3,[7-8,14-22] $M_{5,4}$-,[12,19,23-30] and $N_{5,4}$-edges,[12] as well as ligand K-edges.[31-32] Some of these studies have presented evidence for the importance of both 4f and 5d orbital contributions to covalency in Ce bonding.[15,18,31-36] Extended solids including CeO_2 have also served as important test cases for evaluating whether accurate theoretical methodology can treat the 4f-electrons simply as part of the core, or whether a more demanding approach should be followed that allows the 4f-electrons to delocalize and participate in bonding.[37-46] Cerium intermetallics have been at the forefront of condensed matter physics and development of the Anderson impurity model for heavy fermion systems and Kondo insulators.[47] For example, Ce L_3- and $M_{5,4}$-edge XANES spectroscopic investigations of $CeRu_3$, $CeRh_3$, and $CePt_3$ have provided evidence for 4f-electron delocalization,[20,23,48-49] and L_3-edge investigations of intermetallics such as $CeCoIn_5$ have led to new understanding of their remarkable magnetic and superconducting properties.[50-54] The pace of synthetic, experimental, and theoretical progress has been impeded recently due to sample purity concerns, uncertainty regarding the interpretation of complex spectral phenomena, and the validity of theoretical approximations required to model periodic systems.

From the synthetic perspective, many more molecular Ce^{4+} species can be prepared than the handful of available extended solids.[55-56] Molecular cerium compounds are usually stabilized in the 4+ formal oxidation state by halides[57] and hard, oxygen donor ligands such as alkoxides[58-67] and acetylacetonates.[68-69] Many "non-classical" tetravalent cerium molecules have also been prepared, including organometallic compounds,[70-72] amide,[65,70,73-78] porphyrins[79-83] and a variety of other multidentate N–donor ligands.[84-91] Among these, the lanthanide sandwich molecule cerocene, $(C_8H_8)_2Ce$,[92-103] has played a central role in development of electronic structure models for tetravalent cerium molecules. Theoretical, magnetic, and L_3-edge XANES studies of $(C_8H_8)_2Ce$ resulted in observation of the Kondo effect in a single molecule – a phenomenon that is typically reserved for metals.[96,98] More recently, an in-depth chlorine K-edge X-ray absorption spectroscopy (XAS) and DFT study showed that Cl 3p and Ln 4f covalency was significant in tetravalent $CeCl_6^{2-}$ but virtually nonexistent in the trivalent analog, $CeCl_6^{3-}$.[57]

In spite of this and other notable synthetic progress,[57,72,87,98,104-106] molecular Ce compounds are seldom the subject of emerging methods for physical and theoretical characterization. Molecular solids are promising candidates for further study because they can often be prepared as pure, crystalline compounds, can be designed with high symmetry, and can be modeled as a complete system without requiring periodic boundary conditions or other approximations. Coordination compounds are also desirable for spectroscopic studies because ligand environments can be modified in a systematic fashion. Moreover, recent work has shown that ligand fields can be used to tune lanthanide redox chemistry[65,104-109] and

ground state electronic configurations.[110-115] Clearly, efforts to advance understanding of the roles that covalency and electronic structure play in governing chemical and physical properties would benefit from broader integration of synthetic, spectroscopic, and theoretical research efforts.

In this study, a macrocyclic Ce^{4+} complex was fully characterized in both the solution and solid states to develop a detailed picture of bonding and electronic structure. We have recently described the physical properties of a Th^{4+} specific complex with a macrocyclic ligand (**L**) that incorporates terephthalamide (TAM) binding groups in a macrocycle with pendant arms (Figure 1). [116] The remarkable thermodynamic stability with Th^{4+} has prompted further study of the electronic structure and bonding of Th**L**K_4, and comparisons with the Ce analog, Ce**L**K_4. Developing the chemistry of these ligands is needed to understand their possible applications.[117-119] While lanthanides and actinides can exhibit significantly different chemical behaviors, the use of lanthanides as actinide analogs has enabled the advancement of actinide chemistry and continues to be useful.[120-127] For example, Ce^{4+} and Pu^{4+} have nearly identical ionic radii (0.87 and 0.86 Å, respectively)[128] and similar shifts in the 4+/3+ reduction potentials in aqueous solutions.[129]

Figure 1. Octadentate macrocyclic ligand (**L**H_8) with terephthalamide binding groups. (The free ligand, with unspecified protonation state and charge, will be denoted as **L**. When bound to a metal ion, as in the complex Ce**L**K_4, **L** is fully deprotonated and has a -8 charge.)

The Ce**L**K_4 compounds were characterized in the solid state using single-crystal X-ray crystallography (XRD), and with $M_{5,4}$- and L_3- edge XANES spectroscopic investigations using scanning transmission X-ray microscopy (STXM). In solution, data were obtained from spectrophotometric titrations, and from electrochemical studies of the Ce$\mathbf{L}^{4-}$ system in the context of the absolute stabilities of both the tetravalent and trivalent states of cerium via the measurement of the binding constants between **L** and Ce^{4+} and Pr^{3+}. The comprehensive analysis is generally consistent with established models of bonding for Ce^{4+} compounds; however, the experimental outcomes also diverge in some notable instances.

EXPERIMENTAL SECTION

Synthesis. All chemicals were used as supplied without further purification, unless otherwise noted. Characterization data were obtained at facilities at the University of California, Berkeley. NMR spectra were obtained at room temperature on a Bruker AV-500 spectrometer, with chemical shifts reported in parts per million (ppm) relative to solvent residual signals. Mass spectra were obtained at the QB3/Chemistry Mass Spectrometry Facility, on a Finnigan LTQ FT high-resolution electrospray ionization (ESI) mass spectrometer. Yields indicate the amount of isolated material. **L** was synthesized as previously described.[116]

*Ce**L**K*$_4$. **L**, as the salt **L**H_8·3HCl (23.65 mg, 0.0197 mmol), was suspended in 4 mL methanol in a 10-mL round-bottom flask that had been soaked in an EDTA bath overnight. A solution of $CeCl_3$·$7H_2O$ (Sigma-Aldrich, 7.26 mg, 0.0195 mmol) in 1 mL methanol was added dropwise to the ligand solution

while stirring, resulting in a yellow suspension. A stoichiometric amount of 0.2 M KOH in water (0.985 mL, 0.197 mmol) was added to the ligand suspension dropwise, to a pH of 8, and the reaction mixture immediately became dark purple, indicating the oxidation of Ce^{3+} to Ce^{4+}. The reaction mixture was refluxed under nitrogen flow for 3 h, and once cooled to room temperature, was dropped into 30 mL diethyl ether, producing a fine precipitate. The dark purple precipitate was filtered and dried overnight under vacuum (35.90 mg, 94%). ^{1}H NMR (500 MHz, MeOD) δ 2.33 (dd, *J* = 12.3, 6.6 Hz, 2H, tren CH_2), 2.68 – 2.77 (m, 6H, CH_3), 2.84 (t, *J* = 11.8 Hz, 4H, tren CH_2), 2.87– 2.96 (m, 4H, tren CH_2), 3.24 – 3.51 (m, 14H, tren CH2, methoxyethanamide CH_2), 3.65 (br t, 4H , methoxyethanamide CH_2), 3.99 (d, *J* = 14.3 Hz, 2H, tren CH_2), 6.87 (dt, *J* = 17.1, 7.2 Hz, 6H, Ar H), 7.08 (d, *J* = 8.7 Hz, 2H, Ar H). (-)-HR ESIMS calcd for $C_{50}H_{55}O_{18}N_{10}Ce$ (Ce**L**H^{3-}): 407.7589; found *m/z* 407.7582. Anal. calcd for $C_{50}H_{54}CeK_4N_{10}O_{18}$ ·5KCl·12H_2O: C, 30.51; H, 3.99; N, 7.12. Found: C, 30.76; H, 3.98; N, 7.00.

*Pr**L**K*$_5$. **L**, as the salt **L**H_8·3HCl (20.84 mg, 0.01736 mmol), was suspended in 4 mL methanol in a 10-mL round-bottom flask (that had been soaked in an EDTA bath overnight). A solution of $PrCl_3$·6H_2O (Ventron Alfa Products, 6.07 mg, 0.0172 mmol) in 1 mL methanol was added dropwise to the ligand solution while stirring, resulting in a yellow suspension. A stoichiometric amount of 0.4896 M KOH in methanol (11 equiv.) was added to the ligand suspension dropwise, to a pH of 8, and the reaction mixture gradually became clear and yellow-green. The reaction mixture was refluxed under nitrogen flow for 5 h. Upon cooling to room temperature and precipitation with the addition of 2-5 mL diethyl ether, a light green solid was filtered onto a glass frit. The solid was dried for 6h under vacuum (19.0 mg, 77%). (-)-HR ESIMS calcd for $C_{50}H_{58}O_{18}N_{10}Pr$ (Pr**L**H_4^-): 1227.3063; found *m/z* 1227.3008.

X-Ray Crystallography. A selected crystal of Ce**L**K_4 was mounted in Paratone N oil at the end of a Kaptan loop and frozen in place under a low-temperature nitrogen stream. The data were collected on a Bruker APEX-II CCD X-ray diffractometer with Mo Kα radiation in the X-Ray Facility in the University of California, Berkeley College of Chemistry. Intensity data with a maximum 2θ range of 51.04° were extracted from the frames with the program APEX2. The data were corrected for Lorentz and polarization effects, and an empirical absorption correction was applied using the SADABS program.[130] The structure was solved by direct methods and refined using full-matrix least squares refinements based on *F*2 in SHELXL-97.[131] Crystallographic analyses were performed using the WinGX system of programs.[132] All non-hydrogen atoms were refined anisotropically, while hydrogen atoms were assigned to idealized positions. Disordered solvent molecules were treated with the SQUEEZE procedure included in PLATON. A void of 922 Å^3 containing 287 electrons was found.

Cerium M$_{5,4}$-edge Measurements. STXM methodology was similar to that discussed previously.[133-136] Single-energy images and Ce $M_{5,4}$-edge XANES spectra were acquired using both the STXM instruments at the Canadian Light Source (CLS) spectromicroscopy beamline 10ID-1 and at the Advanced Light Source-Molecular Environmental Science (ALS-MES) beamline 11.0.2. The CLS operated in decay mode (250 to 150 mA) while the ALS operated in topoff mode (500 mA). At both facilities, the beamlines operated with a 0.5 atm He-filled chamber and used elliptically polarizing undulators that delivered photons to entrance slit-less plane-grating monochromators.[137-140] This provides a 130 to 2700 eV working energy range at the CLS, and a 90 to 1950 eV working energy range at the ALS. Energy calibrations were performed at the Ne K-edge for Ne (867.3 eV). The maximum energy resolution *E*/Δ*E* approaches 7,000 for both beamlines,[137-138] which is consistent with the observed standard deviation for spectral transitions of ± 0.1 eV determined from comparison of spectral features over multiple particles and beam runs. For these measurements, the X-ray beam was focused with a zone plate onto the sample, and images at a single energy were obtained by raster-scanning the sample and collecting transmitted monochromatic light with a photomultiplier tube as a function of sample position. Spectra at particular regions of interest on the sample image were extracted from the "stack", which is a collection of images recorded at multiple, closely spaced photon energies across the absorption edge. Dwell times used to acquire an image at a single photon energy were 1 or 2 ms per pixel. To quantify the absorbance signal, the measured transmitted intensity (I) was converted to optical density using Beer−Lambert's law: $OD = \ln(I/I_0) = \mu\rho d$, where I_0 is the incident photon flux intensity, d is the sample thickness, and μ and ρ are the mass absorption coefficient and density of the sample material, respectively. Incident beam

intensity was measured through the sample-free region of the Si_3N_4 windows. Regions of particles with an absorption of >1.5 OD were omitted to ensure the spectra were in the linear regime of the Beer−Lambert law. During the STXM experiment, sample particles of Ce**L**K_4 were homogenous on the micron-scale and did not show signs of radiation damage following data acquisition. Spectra were collected using linearly polarized radiation, and transition energies and intensities were reproduced from multiple independent particles, samples, and beam runs.

In a typical data analysis, a line was fit to the pre-edge region, and then subtracted from the experimental data to eliminate the background of the spectrum. The data were normalized by fitting a first-order polynomial to a 100 eV region of the spectrum beginning approximately +10 eV after the tail-end of the last M_4-edge peak. Derivative spectra were used as guides to determine the number and position of peaks, and edge features were modeled by pseudo-Voigt line shapes and a step function comprised of a 1:1 ratio of arctangent and error function contributions. The first and second derivatives of the data suggested that four pseudo-Voigt functions provided the best fit with the fewest functions. The area under the edge peaks (defined as the intensity) was equal to the fwhm × ph, where fwhm = full width at half maximum height (eV), ph = peak height (normalized intensity). Using the sample preparation methodology discussed above, the reported intensities were reproduced with a standard deviation of less than 10%.

Cerium $L_{3,2}$-edge Measurements. Sample preparation and measurement details are similar to previous work.[98-99] In particular, air-sensitive samples were prepared in an inert atmosphere glove box, where they were ground and mixed with dried boron nitride and sealed in an aluminum multislot holder using aluminized mylar windows and indium seals. The sample holders were then placed in sealed jars for transport. Once at beamline 11-2 at the Stanford Synchrotron Radiation Lightsource, the jars were opened and the sample holders were mounted immediately into a liquid helium flow cryostat for the Ce L_3-edge x-ray absorption measurements. The sample chamber was repeatedly flushed with helium gas and evacuated, and data were collected between 30 and 300 K. The CeO_2 sample was simply ground and brushed onto adhesive tape and measured at room temperature. The incident energy was calibrated such that the peak in the first derivative of the CeO_2 spectrum was set to 5723 eV. In all cases, the amount of sample was chosen such that the change in the absorption at the Ce L_3 edge was below 1 absorption length, generally around 0.3 absorption lengths. The collimating slit height was chosen such that the instrumental resolution was well below the core-hole lifetime-broadened linewidth of about 3.2 eV. [141] Data were collected in transmission mode. All data displayed here have a linear pre-edge subtracted from the data, based on a fit to the pre-threshold absorption. These data are also normalized to the step height as determined by a linear function based on a fit to the data above the edge and then extrapolated back to the edge.

The Ce L_3 data were fit using methods very similar to those described above for the $M_{5,4}$ edge data. In particular, three pseudo-Voigt peaks were used to model resonance features to discrete unoccupied states and an integrated pseudo-Voigt (essentially an arctan function) was used to simulate excitations into the continuum. The main two pseudo-Voigt peaks correspond to the $4f^0$ and $4f^1\underline{L}$ states mentioned above, and a smaller resonance at the foot of the main edge is ascribed to a final state $4f^2$ occupation. The latter resonance is generally quite small and is ignored in the final analysis. The normalized area of the $4f^1\underline{L}$ peak corresponds to the f-occupancy, $n = A_{f1}/(A_{f1}+A_{f0})$. Relative errors in this ratio are generally better than 5%, and absolute errors are better than 10%.

CTM4XAS Calculations. Multiplet calculations were implemented using CTM4XAS, which is a program based on the original code by Cowan[142] and further developed by de Groot.[143] Effects of the crystal field are typically minimal in f-systems, so they were not included.[142] The configurations were defined by 4f-4f Coulomb repulsion (F_{ff}) at atomic values, Coulomb 3d-4f repulsion (F_{fd}) reduced to 40% of atomic values, 3d-4f Coulomb exchange (G_{fd}) reduced to 80% of atomic values, and SOC reduced to 97% of atomic values. For the $3d^94f^1$ configuration this resulted in values of F_{fd} = 2.622, G_{fd} = 3.621, and SOC = 7.219 eV. For the $3d^9\underline{L}4f^2$ configuration this resulted in values of F_{fd} = 2.396, G_{fd} = 3.247, and SOC = 7.223 eV. Additionally, the parameter space was defined by ΔE_{gs} = 1.0 eV, ΔE_{fs} = -1.0 eV, and $T_{gs} = T_{fs}$ = 0.65. A Gaussian broadening of 0.25 eV was applied to account for instrumental broadening and

Lorentzian broadenings of 0.4 and 0.6 eV were applied to the M_5 and M_4 edges, respectively.

Solution Thermodynamics. Thermodynamic stability can be quantitated with the log β_{mlh} value, where β_{mlh} is the cumulative stability constant for the following equilibrium:

$$mM + lL + hH \rightleftharpoons M_mL_lH_h$$

All spectrophotometric titrations were carried out with constant stirring and a blanket of Ar flow in a jacketed cell connected to a recirculating water bath to maintain the temperature at 25°C. The ionic strength of all solutions was maintained at 0.1 M with 0.1 M KCl in titrand solutions and 0.1 M acid and base titrants. A solution of 0.25 N cerium sulfate (Sigma-Aldrich) was used as purchased. A stock solution of Pr^{3+} was prepared by the dissolution of $PrCl_3 \cdot 6H_2O$ (Ventron Alfa Products) in water. The ligand was added as a 50 mM DMSO solution, prepared by dissolution of the solid ligand, weighed on an analytical balance accurate to 0.01 mg. The HCl and KOH solutions were prepared by dilution of Dilut-It (J.T. Baker, ampoules) concentrated solutions with degassed Millipore water. The 0.1 M HCl solution was standardized by the potentiometric titration of tris(hydroxymethyl)aminomethane, and the 0.1 M KOH solution was standardized by potentiometric titration of potassium hydrogen phthalate or the standardized HCl solution. The KOH solution was stored under a blanket of Ar flow and standardized before every titration. The glass electrode (Metrohm Microtrode or Orion Pinnacle) used for the pH measurements was calibrated by the titration of 1.000 mL standardized 0.1 M HCl in 25.0 mL 0.1 M KCl with standardized 0.1 M KOH to pH 11.6. The titration was analyzed using the program GLEE to refine for E° and the slope.[144] This calibration was also performed prior to each titration. The automated titration system was controlled by a Metrohm Titrando 907 and the program Tiamo® light. 2 mL Dosino 800 burets dosed the titrant into the titration vessel (5-90 mL). UV-Vis spectra were acquired with an Ocean Optics USB4000-UV-Vis spectrometer equipped with a dip probe (set to a 10 mm path length) and a DH-2000 light source (deuterium and tungsten lamps), using the program Spectra Suite. Some titrations were also performed using Metrohm Brinkmann 665 Dosimat automated burettes, a Fisher Accumet AR 15 pH meter, and a Hewlett-Packard 8452A UV-Vis spectrometer (orchestrated through the interface of the computer program Labview). Titrations were performed at least in triplicate.

*Ce^{4+} **L** Competition Titration.* 20 mL solutions of 50 µM **L**, 50 µM $Ce(SO_4)_2$, 1 mM NTA (Eastman Organic Chemicals) were titrated forward and backward with between pH 2.9 and 10.0 with 0.1 M KOH and 0.1 M HCl. 1 mM MES and 1 mM HEPES were used to buffer the system, which was maintained at an ionic strength of 0.1 M with KCl. The Ce^{4+} was added to a solution of NTA and buffer, and this clear, light yellow solution was allowed to equilibrate for at least 24 h prior to the addition of ligand and used as the blank spectrum. The data points (pH readings and UV-Vis spectra) were collected at approximately 0.4 pH increments, with an equilibration time of 10 min following KOH additions (forward titrations) or 20 min following HCl titrations (backward titrations). 0.1 M HCl was added to the solution prior to the forward titration to reach the starting pH. All absorbance measurements used in the refinement were no larger than 1.1 absorbance units. Spectra of 280-800 nm were analyzed (simultaneously) in the program Hypspec.[145-146] The following values for the log β for the formation of cerium hydroxides were included in the refinement: $[CeOH]^{3+}$, -0.56; $[Ce_2(OH)_3]^{5+}$, -0.44; $[Ce_2(OH)_4]^{4+}$, -0.62; $[Ce_6(OH)_{12}]^{12+}$.[147] The following protonation and stability constants for NTA and the $Ce(NTA)_2$ complex were utilized: log β_{011}, 9.84; log β_{012}, 12.36; log β_{013}, 14.17; log β_{014}, 15.17; log β_{120}, 38.6.[148] Spectra and protonation constants of the free ligand, refined from previously determined ligand titrations,[116] were set constant in the refinement and pM values were determined using the program Hyss.[149]

*Pr^{3+} **L** Titration.* 20 mL solutions of 50 µM **L** and 50 µM $PrCl_3$ were titrated forward and backward with between pH 2.6 and 11.0 with 0.1 M KOH and 0.1 M HCl. 1 mM each of MES, HEPES, and CHES were used to buffer the system, which was maintained at an ionic strength of 0.1 M with KCl. The data points (pH readings and UV-Vis spectra) were collected at approximately 0.4 pH increments, with an equilibration times of 10 min. 0.1 M HCl was added to the solution prior to the forward titration to reach the starting pH. All absorbance measurements used in the refinement were no more than 1.1 absorbance units. Spectra of 250-450 nm were analyzed (simultaneously) in the program Hypspec. The following

value for the log β for the formation of praseodymium hydroxide was included in the refinement: $[PrOH]^{2+}$, -7.1.[150] Spectra and protonation constants of the free ligand, refined from the ligand titrations, were set constant in the refinement.

Electrochemistry. Cyclic voltammograms were obtained using a three-electrode system (hanging drop mercury working electrode, silver/silver chloride reference electrode, platinum wire auxiliary electrode) and an EC-Lab SP-200 potentiostat. Nine drops of electrochemical grade mercury (used as purchased) were grown at the capillary for each measurement. A resistance correction was applied to the cyclic voltammograms using the resistance measurement of the electrolyte solution. Sample solutions were prepared by dissolving the solid isolated complex Ce**L**K_4 into aqueous 1 M KCl, to a concentration of 1 mM. Solutions were purged with argon flow prior to each scan and kept under a blanket of argon during scans.

RESULTS AND DISCUSSION

Structural Characterization of Ce$\mathbf{LK_4}$**.** The Ce**L**K_4 complex was synthesized by reaction of the ligand with a Ce^{3+} source, followed by deprotonation with base and oxidation by atmospheric oxygen. Single crystals suitable for XRD were grown by the vapor diffusion of diisopropyl ether into a 1:4::DMF:MeOH solution of the isolated potassium salt of the Ce^{4+} complex (Figure 2). Other than for the shorter Ce-O bond lengths (Ce^{4+} has an ionic radius of 97 pm, whereas that of Th^{4+} is 105 pm),[128] the crystal structure of the Ce complex was directly analogous to that of the Th complex[116] in space group, unit cell, and inner coordination environment (Table 1). As with the Th^{4+} ion, the ligand does not maintain its symmetry when bound to the Ce^{4+} center in the solid state. Instead of adopting the C_{2h}-symmetric conformation of the free ligand, it displayed a pseudo-C_2 symmetry where the pendant TAMs are adjacent to one another, and on the same side of the macrocyclic TAMs, which are offset from the metal ion equator.

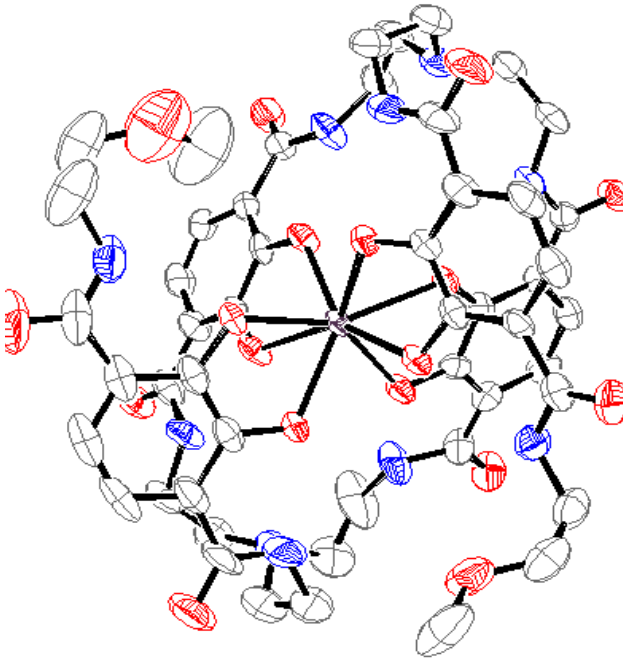

Figure 2. ORTEP[151] diagram of the Ce$\mathbf{L}^{4-}$ complex. Ellipsoids are shown at 50% probability. Hydrogen and potassium atoms are omitted for clarity (gray C, red O, blue N, violet Ce).

Table 1. Crystallographic data and structure refinement for Ce**L**K_4.

Empirical formula	$C_{50}H_{54}CeK_4N_{10}O_{18}$	
M_r	1379.05 g/mol	
Temperature	100(2) K	
Wavelength	0.71073 Å	
Crystal system	Triclinic	
Space group	*P*T	
Unit cell dimensions	a = 11.3510(7) Å	α = 79.136(2)°
a	b = 16.4110(12) Å	□ = 86.923(2)°
	c = 20.1170(14) Å	□ = 80.584(2)°
V	3632.1(4) Å^3	
Z	2	
□$_{calcd}$	1.261 mg/m^3	
μ_{calcd}	0.919 mm^{-1}	
F (000)	1403	
Crystal size	1.00 x 0.03 x 0.01 mm	
2□ range for data collection	1.49 to 25.52°	
Index ranges	-13<=h<=13, -19<=k<=19, -23<=l<=24	
Reflections collected	25169	
Independent reflections	12747 [R(int) = 0.0316]	
Completeness to □ = 25.00°	95.3 %	
Absorption correction	Semi-empirical from equivalents	
Max. and min. transmission	0.9909 and 0.4601	
Refinement method	Full-matrix least-squares on F^2	
Data / restraints / parameters	12747 / 29 / 760	
Goodness-of-fit on F^2	1.134	
Final R indices [$I > 2\sigma(I)$]	$R1$ = 0.0815, $wR2$ = 0.2353	
R indices (all data)	$R1$ = 0.1036, $wR2$ = 0.2614	
Largest diff. peak and hole	5.405and -0.872 e.Å^{-3}	

Solution Thermodynamics. The dark purple color of the Ce**L**$^{4-}$ complex renders the measurement of its stability constant by spectrophotometric titration especially practicable (Figure 3). Due to the remarkable stability of the ligand with Th^{4+}, we predicted that the ligand would also have a high affinity for the lanthanide analog. This necessitated the use of a competing ligand; nitrilotriacetic acid (NTA) was used because it forms a colorless and highly stable complex with Ce^{4+}. Its log β_{120} of 38.6(8)[148] makes it a better competitor for Ce^{4+} than the commonly-used DTPA, which has a lower log β_{110} value.

The formation of the Ce**L**$^{4-}$ complex could be monitored by both the shift of the ligand deprotonation to a lower pH (Figure 4a) and the appearance of the ligand-to-metal charge transfer (LMCT) centered at 522 nm (Figure 3, 4b). As with Th^{4+} titrations, the main equivalence point observed corresponds to the deprotonation of the Ce**L**H^{3-} to the Ce**L**$^{4-}$ species, the refined spectrum (Figure 5) of which correlates well with that of the isolated synthesized complex. Refinement of the NTA competition titrations gave a log β_{110} = 61(2) and a pK_a = 5.5(7) (Table 2). The rather large standard deviations of these values are partly due to the errors in the NTA stability constant and **L** protonation constants; moreover, the measurement of such a high affinity is inherently uncertain.

The stability of Ce**L**$^{4-}$ is 20 orders of magnitude greater than that of the Ce^{4+} complex with the hydroxypyridinone ligand 3,4,3-LI-1,2-HOPO, whose stability constant of log β_{110} = 41.5(2) was among the highest measured for Ce^{4+}.[152] This thermodynamic stability surpasses that of the Th**L**$^{4-}$ complex by over seven orders of magnitude, which is attributable to the greater charge-to-radius ratio of Ce^{4+} relative

to Th^{4+} (Table 2). The same trend is present with DTPA, which is more stable with Ce^{4+} than Th^{4+} by five orders of magnitude.

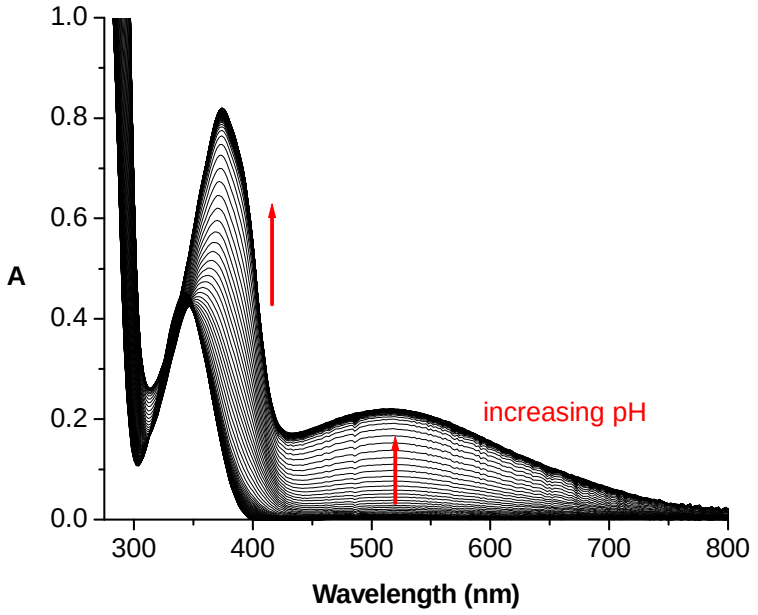

Figure 3. UV-Vis spectra of spectrophotometric competition titration of Ce**L**$^{4-}$ with NTA. Starting conditions: 50 µM Ce^{4+}, 50 µM **L**, 1 mM NTA, 1mM MES, 1mM HEPES, and 0.1 M KCl (25°C). *A* vs. wavelength plot at varying pH values.

Table 2. Stability Constants and pM Values for Complexes with **L** and DTPA.

Metal ion	Charge-to-radius ratio ($Å^{-1}$),[16] CN = 8	**L**[a]		DTPA[b]	
		Log β_{110}, log *K*s	pM	Log β_{110}, log *K*s	pM
Pr^{3+}	2.66	32.02(2), 8.1(2), 7.0(2)	18.0	21.10, 2.38	17.6
Th^{4+}	3.81	53.7(5), 5.2(2)	39.1	28.78, 2.16	26.8
Ce^{4+}	4.1	61(2), 5.5(7)	46	34.04	30.59

[a]Values for Th^{4+} from ref. 30
[b]Values for Th^{4+} and Ce^{4+} from ref. 61, values for Pr^{3+} from ref. 45.
pM = $-\log[M]_{free}$; $[M]_{tot} = 10^{-6}$ M, $[L]_{tot} = 10^{-5}$ M

a)

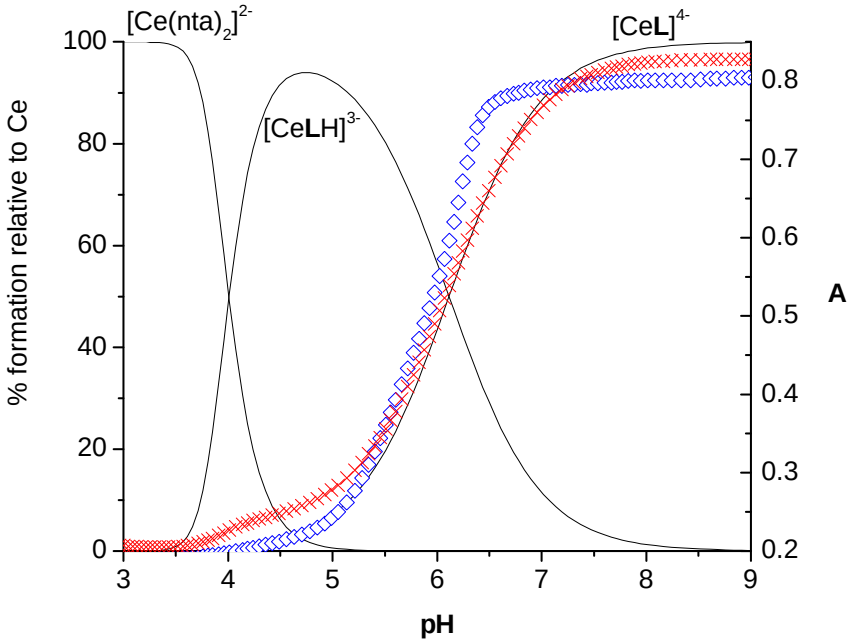

b)

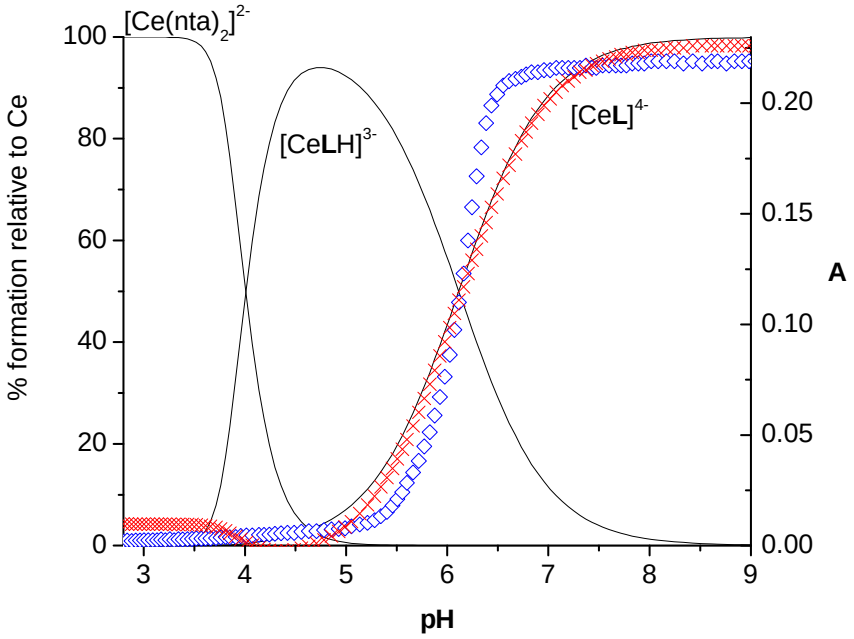

Figure 4. Plots of *A* (absorbance) vs. pH of spectrophotometric competition titration of Ce**L**$^{4-}$ with NTA. Starting conditions: 50 μM Ce^{4+}, 50 μM **L**, 1 mM NTA (nta), 1mM MES, 1mM HEPES, and 0.1 M KCl (25°C). *A* vs. pH at (a) 370 nm, the λ_{max} of the ligand $\pi \rightarrow \pi^*$ transition, and (b) 522 nm, the λ_{max} of the LMCT band, (experimental data points are blue diamonds, red crosses are calculated absorbances) overlaid onto speciation.

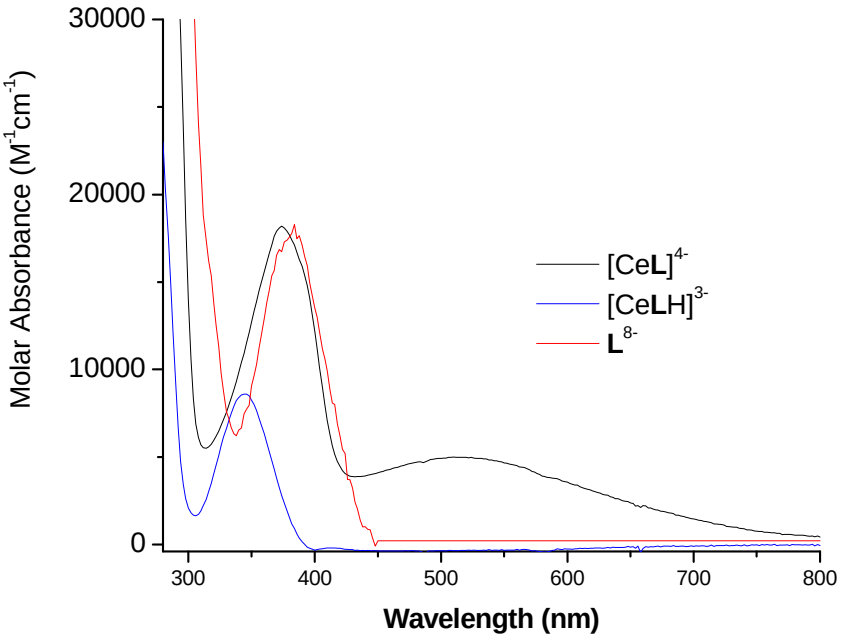

Figure 5. Molar absorbances of Ce**L**$^{4-}$ and Ce**L**H^{3-} and the fully deprotonated **L**.

The thermodynamic stability of TAM ligands for Ln^{3+} ions has been measured in six-coordinate complexes—gadolinium complexes for applications in MRI contrast agents—but not for eight-coordinate complexes. An analog for **L** is the hexadentate ligand TREN-TAM$_3$, which has a log β_{110} > 17 with Gd^{3+}.[153] Even though **L** has the same TAM binding units, it is difficult to predict its stability with a +3 lanthanide ion given the difference in coordination number and the entirely different topology of the ligands. To obtain a quantitative assessment of the selectivity of **L** for +4 over +3 metal ions, its stability with an Ln^{3+} ion was investigated as a surrogate for Ce^{3+}.

The direct verification of a Ce(+4/+3) redox potential shift due to complexation by the independent measurement of the Ce^{3+} stability constant was not possible due the overwhelming preference of Ce**L**$^{4-}$ for the +4 oxidation state. Even by excluding oxygen from the titration cell as much as possible, titrations with Ce^{3+} resulted in its oxidation to Ce^{4+} upon complexation. Based on ionic radii comparisons, Pr^{3+} is a closer analog to Ce^{3+} than Gd^{3+}, and spectrophotometric titrations with Pr^{3+} and **L** were then performed (Figure 6a). The shift in the ligand deprotonation to lower pH values, indicative of complexation, was accompanied by two main equivalence points (Figure 6b). This was refined to a model describing the formation of two dominant species in solution, the mono- and di-protonated praseodymium complexes with log β_{110} = 32.02(2) and pK_{a1} = 8.1(2) and pK_{a1} = 7.0(2) (the refined individual spectra are shown in Figure 7). The M**L**H$_2$ species is observed with Pr^{3+} but not with Ce^{4+} or Th^{4+} most likely because of the greater negative charge of the complex with Pr.

The binding affinity of **L** for Pr^{3+} is considerably greater than that of DTPA but its pM value is about the same (Table 2), indicating that it is not an exceptional chelator for the sequestration of cations with low charge-to-radius ratios like Ln^{3+} and An^{3+} ions. The 29-order magnitude difference in binding constants between Pr^{3+} and Ce^{4+} is indicative of a very strong preference for Ln^{4+} and An^{4+} ions, a property that would be advantageous in selective sequestration applications.

The high affinity of **L** for Ce^{4+} is attributable to the impact of charge-to-radius ratio on the stability of complexes with hard catecholate donors. The binding constant of **L** increases with increasing charge-to-radius ratios (Ce^{4+}, Pr^{3+} and Th^{4+}; Table 2). While the relationship between charge-to-radius ratio and metal ion affinity has previously been observed, such a large difference in stability between analogous Ce^{4+} and Th^{4+} complexes is extremely unusual, if not unprecedented. [119,152]

a)

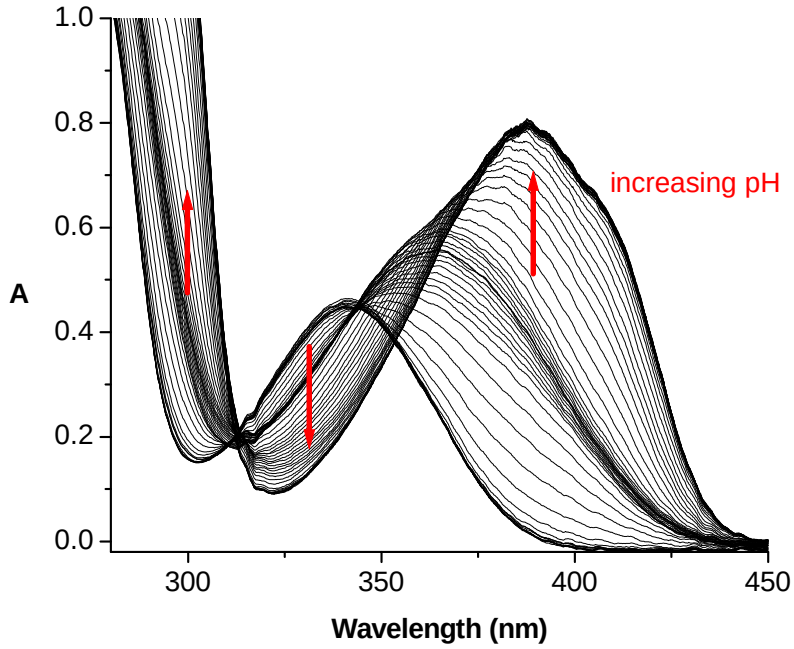

b)

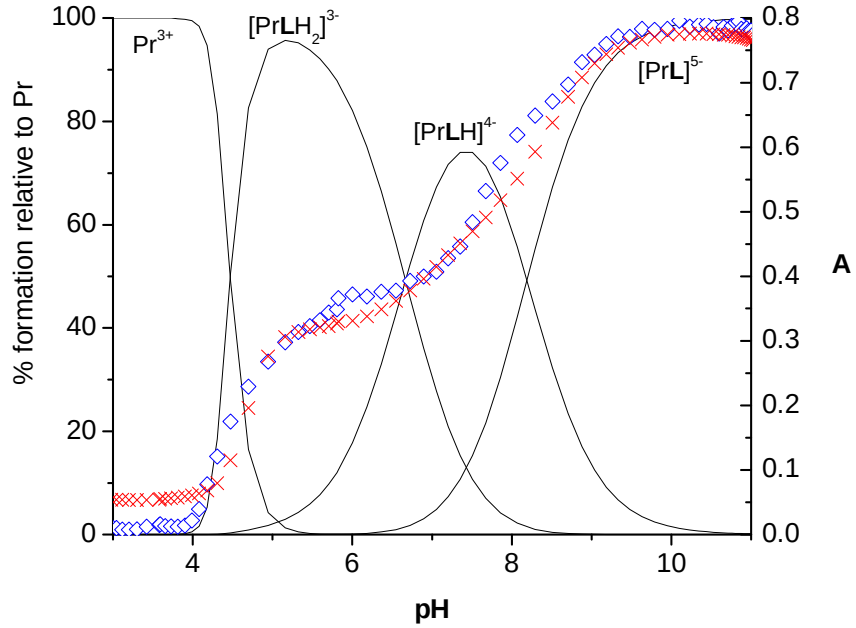

Figure 6. Spectrophotometric titration of Pr**L**$^{5-}$. Starting conditions: 50 μM Pr(III), 50 μM **L**, 1 mM MES, 1mM HEPES, 1 mM CHES and 0.1 M KCl (25°C). a) *A* vs. wavelength plot at varying pH (data abridged for clarity; spectra normalized for dilution). b) *A* vs. pH at 390 nm (experimental data points are blue diamonds, red crosses are calculated absorbances) overlaid onto speciation.

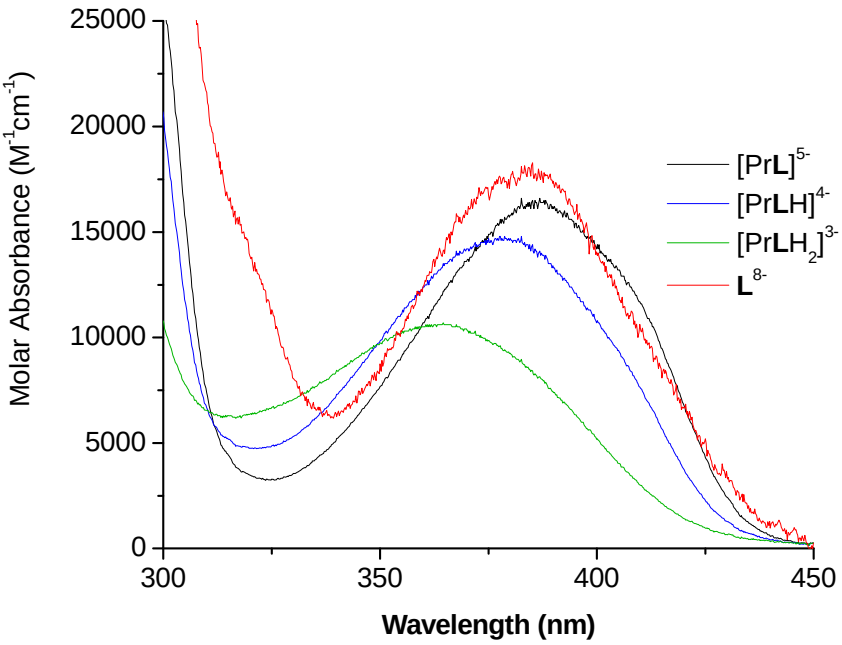

Figure 7. Molar absorbances of species of Pr**L**$^{5-}$ and the fully deprotonated **L**.

Ce L_3-edge and $M_{5,4}$-edge XANES Spectroscopy. Considering the remarkable affinity of macrocyclic ligand **L** towards the Ce^{4+} ion, we sought to determine if aspects of the enhancement in metal–ligand bonding are reflected by Ce L_3- and $M_{5,4}$-edge XANES spectroscopies. Both spectroscopic approaches probe electric-dipole allowed transitions from Ce core orbitals to valence orbitals that can participate in ligand bonding, described by

$$2p^6 4f^n 5d^0 \rightarrow 2p^5 4f^n 5d^1 \text{ } (L_3\text{-edge})$$

and

$$3d^{10} 4f^n \rightarrow 3d^9 4f^{n+1} \text{ } (M_{5,4}\text{-edge})$$

where n = the number of 4f electrons in the ground state. Although the excited states probed by L_3-edge and $M_{5,4}$-edge XANES have very different electronic configurations, recent studies have proposed that both are sensitive to 4f orbital occupation.[7,12,17-19,22,24-26,154-157] However, the role of final state effects including core-hole induced changes in 4f occupancy, and other physical phenomena, remains controversial and is the subject of a persistent debate.[18,33,35-36]

Figure 8 compares the background-subtracted and normalized Ce L_3-edge XANES spectra of Ce**L**K_4 and reference compounds CeO_2,[158] $[Et_4N]_2[CeCl_6]$,[57] and $(C_8H_8)_2Ce$.[99] Each of the L_3-edges exhibited a double-peak structure that is characteristic of published data for formally Ce^{4+} compounds such as CeO_2, $Ce(SO_4)_2$, and CeF_4.[7,17-18] The double-peak structure observed in Ce L_3-edge XANES spectra is often taken to reflect the presence of a configuration interaction of the main, ionic $4f^0$ configuration and a LMCT configuration, $4f^1\underline{L}$, where $\underline{L}$ represents a ligand hole. Differences in screening of the 2p core hole by the 4f orbitals results in the large splitting between $4f^1\underline{L}5d^1$ and $4f^05d^1$ final states that is observed in the L_3-edge spectra. Within the bounds of this model, the lower energy peak was assigned to transitions associated with a $4f^1\underline{L}5d^1$ final state and the higher energy peak to transitions involving a $4f^05d^1$ final state, however, the possibility of a more complex excited state phenomenon cannot be ruled out.

For the compounds compared in this study, the peak maxima as determined from zero-crossing of the first derivative of the L_3-edge spectra indicated that there are significant differences in the relative energies of the low and high energy peaks. The first peak corresponding to the $4f^1\underline{L}5d^1$ final state configuration shifted to lower energy from 5728.4 to 5727.3 to 5727.2 to 5724.5 eV on moving from CeO_2 to $[Et_4N]_2[CeCl_6]$ to Ce**L**K_4 to $(C_8H_8)_2Ce$. The energy of the second peak did not change as significantly, such that splittings between transitions associated with the $4f^1\underline{L}5d^1$ and $4f^05d^1$ final state configurations of 7.0, 7.7, 7.8, and 11.1 eV were observed for CeO_2, $[Et_4N]_2[CeCl_6]$, Ce**L**K_4, and $(C_8H_8)_2Ce$. This trend is also supported by examination of the peak intensities. Ce L_3-edge peak structure for Ce**L**K_4 was fitted and a value of n = 0.49(3) 4f electrons was determined by evaluating the intensity ratio of the two peaks together with an arctan-like function to simulate the transitions to the continuum (see Supporting Information). As described above, the quantity n refers to the number of 4f electrons in the ground state defined in a configuration interaction model, and is different from mixing coefficients used in a molecular orbital model. Despite the obvious differences between their spectra, this value of n was found to be statistically identical for $[Et_4N]_2[CeCl_6]$[57] and CeO_2[7,158], respectively, with the values of 0.51(5) and 0.53(5), which are considerably smaller than the value of 0.89(3) reported for $(C_8H_8)_2Ce$.[98]

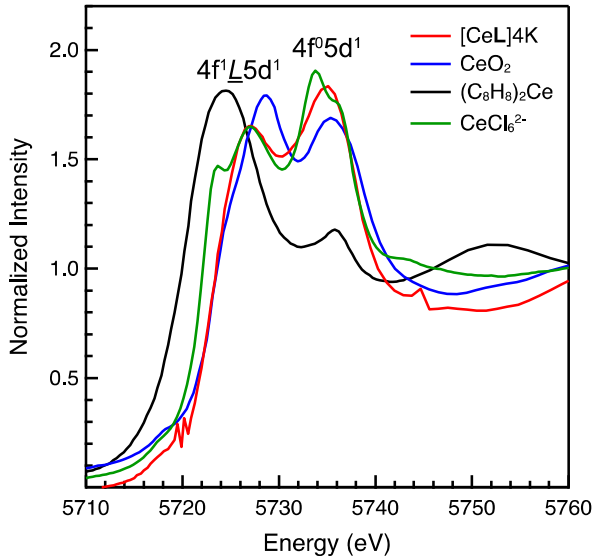

Figure 8. Cerium L_3-edge XANES spectra for Ce**L**K_4 and references CeO_2, COT_2Ce, and $[Et_4N]_2[CeCl_6]$. The $[Et_4N]_2[CeCl_6]$ data are adapted with permission from ref. 19. Copyright 2015 American Chemical Society.

XANES spectra at the $M_{5,4}$-edge were obtained to corroborate the $L_{3,2}$-edge measurements. Transitions at the $M_{5,4}$-edge probe the 4f orbitals directly via 3d to 4f transitions, and the spectra exhibit characteristic multiplet splitting patterns that have been used to assign nominal 4f orbital occupancies across the lanthanide series.[12,18,25] The background subtracted and normalized $M_{5,4}$-edge XANES spectrum and curve fit for Ce**L**K_4 is provided in Figure 9 and compared with published data for $[Et_4N]_2[CeCl_6]$.[159] The $M_{5,4}$-edge XANES spectra are split by approximately 17 eV into M_5 ($3d_{5/2}$) and M_4 ($3d_{3/2}$) due to spin-orbit coupling with the core hole. For pure $4f^0$ compounds (e.g., La^{3+}), $M_{5,4}$-edge XANES spectra are comprised of one peak each for the M_5- and M_4-edges.[25] However, for Ce**L**K_4 both the M_5 and M_4 edges exhibited fine structure consisting of intense main peaks and weaker "satellite" features at 4 to 5 eV higher energies. Previous calculations have attributed the presence of fine structure in the $M_{5,4}$-edge XANES spectra of formally tetravalent Ce compounds to interaction of $3d^94f^1$ and $3d^9\underline{L}4f^2$ configurations in the

final state.[12,36] In this general sense the $M_{5,4}$-edge XANES spectrum of Ce**L**K_4 resembled that of the molecular compound $(Et_4N)_2CeCl_6$ in addition to extended solids and intermetallics such as CeO_2 and $CeRh_3$.[24]

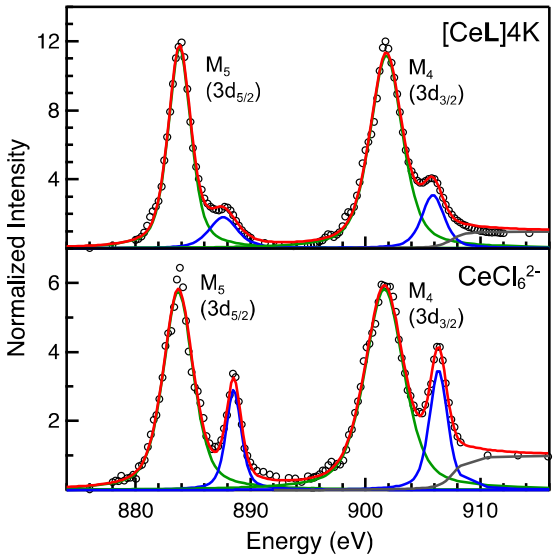

Figure 9. Cerium $M_{5,4}$-edge XANES spectra obtained using STXM for Ce**L**K_4 and $[Et_4N]_2[CeCl_6]$. The data (black circles) are shown with pseudo-Voigt functions (green, blue) and a step function (gray) used to generate the total curve fit. The $[Et_4N]_2[CeCl_6]$ data are adapted with permission from ref. 19. Copyright 2015 American Chemical Society.

Table 3. Comparison of the experimental cerium $M_{5,4}$-edge XANES peak energies and intensities for Ce**L**K_4 and standards CeO_2 and $[Et_4N]_2[CeCl_6]$.

Peak Energies (eV)		Peak Intensities (Int)		Branching Ratio[a]		Peak Splitting (eV)		
M_5-edge	M_4-edge	M_5-edge	M_4-edge	$A_5/(A_5+A_4)$	$A_S/(A_M+A_S)$	Sat–Main	M_5–M_4	Ref
				Ce**L**K_4				
883.8, 887.6	901.8, 905.9	27(3), 5.3(5)	37(4), 7.2(7)	0.42(4)	0.16(2)	3.9	18.0	This work
				CeO_2				
883.7, 888.8	901.7, 906.3	16(2), 4.2(4)	20(2), 5.6(6)	0.44(4)	0.21(2)	4.8	18.0	30
				$[Et_4N]_2[CeCl_6]$				
883.7, 888.5	901.6, 906.4	18(2), 4.5(5)	23(2), 6.5(7)	0.43(4)	0.21(2)	4.8	17.9	15

[a] Branching ratios are determined from the peak intensities (areas), such the A_5, A_4, A_S, and A_M are defined as the area underneath M_5, M_4, satellite, and main features, respectively.

To quantify this effect, peaks in the experimental spectra were modeled using pseudo-Voigt functions and a step function with 1:1 ratio of arctangent and error function contributions (Figure 9 and Table 3). The first and second derivatives of the data suggested that four pseudo-Voigt functions provided the best fit with the fewest parameters (or number of peaks). Hence the main peaks were modeled with functions at 883.6 eV and 901.4 eV, and the satellite peaks were modeled with functions at 887.6 eV and 905.5 eV. The splitting between main and satellite peaks averaged 4.0 eV, which is significantly smaller than the

splitting previously observed for $[Et_4N]_2[CeCl_6]$ (4.9 eV) and CeO_2 (4.8 eV).[57,158] In addition, the satellite-to-main peak intensity ratio was 0.16(2) compared with 0.21(2) for both $[Et_4N]_2[CeCl_6]$ and CeO_2 (Table 3). Calculations by Kotani and coworkers have previously noted that decreasing interaction of the $3d^9\underline{L}4f^2$ and $3d^94f^1$ final states resulted in smaller satellite-to-main peak intensity ratios as well as smaller main-to-satellite peak splittings,[12] suggesting that there is less final state interaction in Ce**L**K_4 compared with $[Et_4N]_2[CeCl_6]$. Thus, the $M_{5,4}$-edge XANES peak structure is partially a reflection of core-hole induced charge-transfer in the final state.

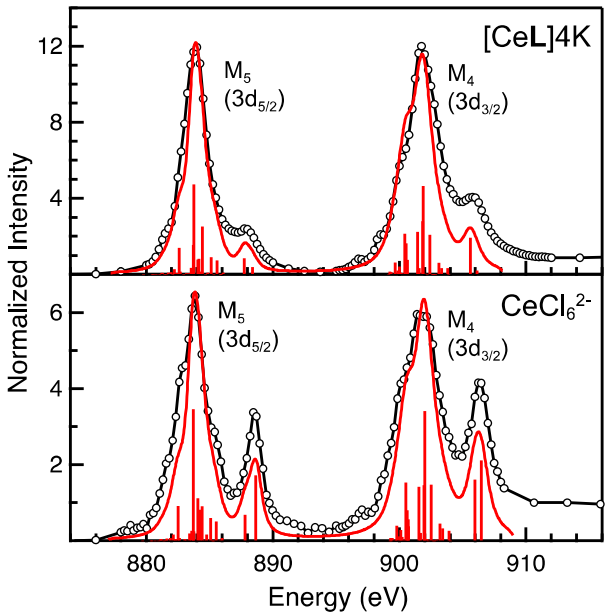

Figure 10. Comparison of the experimental (black circles) and the configuration interaction calculation (red) for the cerium $M_{5,4}$-edge XANES spectra obtained for Ce**L**K_4 and $[Et_4N]_2[CeCl_6]$. The $[Et_4N]_2[CeCl_6]$ data are adapted with permission from ref. 19. Copyright 2015 American Chemical Society.

To explore this result further, configuration interaction (CI) calculations were conducted using the CTM4XAS program, which employs a semiempirical approach developed by de Groot and based on Cowan's code (Figure 10).[142-143,160] This approach has been applied successfully to model and develop quantitative interpretations of charge transfer and multiplet interactions in other transition metal and cerium systems.[161-163] In free-ion systems for which a transition from $3d^{10}4f^0$ to $3d^94f^1$ states does not accurately model the spectra, both the initial and final states can be described in a charge transfer model. In the charge transfer model, both the initial and final states are defined by two configurations, one of which includes a ligand hole ($\underline{L}$) resulting from charge transfer. Thus, the initial state is described by $3d^{10}4f^0$ and $3d^{10}\underline{L}4f^1$ and the final state by $3d^94f^1$ and $3d^9\underline{L}4f^2$. These configurations were defined by 4f-4f and 3d-4f Coulomb repulsion, Coulomb exchange and spin-orbit-coupling (SOC) parameters. The interactions of these states were described by the energy separation of the initial (ΔE_{gs}) and final states (ΔE_{fs}) as well as the mixing of each, T_{gs} and T_{fs} respectively. As described previously,[57] the energy of the lowest LMCT band in the UV/Vis spectrum (2.4 eV) was used to provide bounds for these parameters as governed by LMCT $\approx \Delta E_{gs} + 2T_{gs}$. In addition, the experimentally observed splitting and intensity ratios between the main and satellite peaks in the $M_{5,4}$-edge XANES spectra provided limits for the calculations. The calculations that were in the closest agreement with these experimental data were defined with ΔE_{gs} = 1.0 eV, ΔE_{fs} = -1.0 eV, and $T_{gs} = T_{fs}$ = 0.65, resulting in a ground state that was 62% $3d^{10}4f^0$ and 38%

$3d^{10}\underline{L}4f^1$, and a calculated LMCT of 2.44 eV. For comparison, a ground state composition of 75% $3d^{10}4f^0$ and 25% $3d^{10}\underline{L}4f^1$ was found previously to model the LMCT energy (3.3 eV) for $(Et_4N)_2CeCl_6$ as defined by ΔE_{gs} = 2.5 eV, ΔE_{fs} = -1.5 eV, and $T_{gs} = T_{fs}$ = 0.70.[57] Hence, the CTM4XAS calculations suggest that there is slightly more $4f^1$ character in the ground state of Ce**L**K_4 (38%) than in $(Et_4N)_2CeCl_6$ (25%). The relatively low percentages of $4f^1$ character observed for these two compounds suggested that the LMCT configuration has a smaller contribution to the ground state than previously reported for $(C_8H_8)_2Ce$, based on L_3-edge XANES spectroscopy (89%) and multiconfiguration interaction calculations (80%).[96,164] To summarize, the experimental Ce L_3-edge and $M_{5,4}$-edge XANES measurements and CTM4XAS calculations all provide evidence for some mixing between the Ce 4f and ligand O 2p orbitals, as evidenced by **L** → Ce charge transfer contributions in the ground state. Within the bounds of an oxidation state formalism, Ce**L**K_4 is best regarded as tetravalent with a degree of covalency that is similar to compounds such as CeO_2 and $[Et_4N]_2[CeCl_6]$, but less than that of $(C_8H_8)_2Ce$. Additional $L_{3,2}$- and $M_{5,4}$-edge measurements and theoretical studies on a wider range of molecular Ce compounds would promote a further understanding of orbital contributions to cerium bonding.

Electrochemistry. As a complement to the solution thermodynamic studies with Pr^{3+}, cyclic voltammetry was used to access a complexed Ce^{3+} species. The abundance of literature precedent describing the successful measurement of the redox potential of the Ce^{4+}/Ce^{3+} couple of complexes with a variety of ligands, including catechols,[55,152,165-168] belied the difficulty with which the electrochemical behavior of this system could be probed with a glassy carbon electrode. Reduction and subsequent oxidation of the Ce$\mathbf{L}^{4-}$ complex was successfully observed only with a hanging drop mercury electrode (HDME). Cyclic voltammograms demonstrating nearly reversible behavior at scan rates of 250-2000 mV/s were obtained for the system (as an aqueous solution of the isolated complex) in 1 M KNO_3 (Figure 11a) and in 1 M KCl. The current intensities at cathodic peaks were linearly proportional to the square root of the scan rate, suggesting a diffusion-limited process (Figure 11b), as predicted by the Cottrell equation. The redox behavior of this system was not fully reversible for several reasons (Table 4). The voltage separation between the current peaks was greater than 59 mV but sufficiently close to the ideal value to estimate that a one-electron process was occurring at the metal center. Secondly, the positions of the cathodic and anodic peak voltages changed with increasing scan rates, shifting to more reductive and oxidative potentials, respectively. This effect has been attributed to the slow equilibrium at the electrode surface relative to the higher scan rates.[169] Additionally, the ratio of the peak currents was greater than one, with the cathodic current intensity consistently greater than the anodic current. This was possibly due to the lower stability of the reduced cerium complex, and thus its greater susceptibility to side reactions. At 100 mV/s, the oxidation was not even observed.

The reversibility of the system using the HDME working electrode was sufficient to calculate a redox potential of -0.454 V vs. SHE, a value considerably lower than the potential for uncomplexed Ce^{4+} (1.46 V vs. SHE, in HCl).[170] This very large Nernstian shift of 1.91 V explains the overwhelming preference of the +4 oxidation state of cerium when it is complexed by **L**. Unsurprisingly, the potential of Ce$\mathbf{L}^{4-}$ is close to that of the Ce(catecholato)$_4^{4-}$ complex (-0.448 V vs. SHE),[166] and smaller Nernstian shifts have been observed with octadentate ligands and Ce^{4+},[152,171] but this is the first measure of the Ce couple with an octadentate catecholate-type ligand.

As depicted by a thermodynamic cycle (Figure 12), the electrochemical and solution thermodynamic data for the Ce^{4+} complex can be used to calculate the binding constant between **L** and Ce^{3+}. The estimated log β_{110} = 28.6 is reasonably close to the measured log β_{110} = 32.02 for Pr^{3+}; the discrepancy perhaps demands the direct measurement of the Ce^{3+} complexation. However, it would be surprising that the difference in ionic radii of the Ce^{3+} and Pr^{3+} (114 and 113 pm, respectively) [128] would result in an increased binding affinity of three orders of magnitude; it is more likely that the quasi-reversible electrochemical behavior of the Ce$\mathbf{L}^{4-}$ system requires further investigation.

The thermodynamic cycle can nevertheless be useful in estimating the magnitude of stabilization of the +4 oxidation states of metal ions with similar characteristics as Ce^{4+}. For example, the aqueous reduction potential of the americium +4/+3 couple is estimated to be 2.62 V,[172] which means that Am^{4+} oxidizes water or most other ligands. From the data obtained with the Ce$\mathbf{L}^{4-}$ system and the Nernst

equation (Eq. 1, where $E^{c}_{n/n-1}$ and $E_{n/n-1}$ are the redox couples of the complexed and uncomplexed metal, respectively):

$$E^{c}_{n/n-1} = E_{n/n-1} + (RT/F)\,(\ln K_M{}^{n-1}{}_L - \ln K_M{}^{n}{}_L) \qquad \text{(Eq. 1)}$$

it can be approximated that complexation by **L** would change this potential to 0.95 V. This would make Am^{4+} stable under aqueous conditions, which has not yet been experimentally observed.

a)

b)

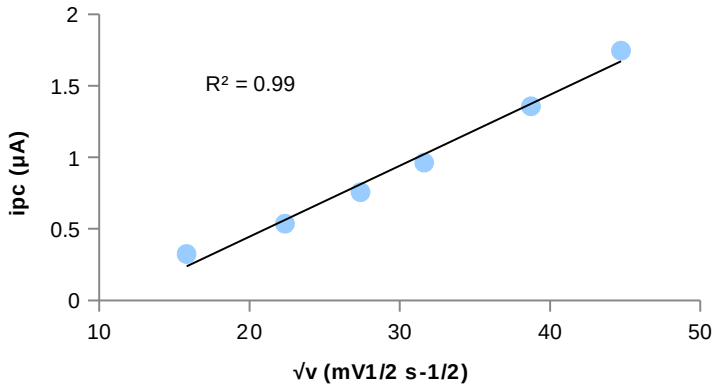

Figure 11. CV of Ce**L**K_4 in 1 M KCl using an HDME working electrode in a three-electrode system. a) Cyclic voltammograms of 1 mM Ce**L**K_4 at scan rates of 100-2000 mV/s, initial scan direction: cathodic. Background taken at 100 mV/s. (b) Linear dependence of the current intensity at cathodic peak current (-0.685 V) vs. the square root of the scan rate.

Table 4. CV data for the Ce$\mathbf{L}^{4-}$ complex in 1M KCl using a HDME working electrode. Values are averages from scan rates of 250-2000 mV/s.

$E_{1/2}$ (V)	-0.651(9) vs. Ag/AgCl -0.454 vs. SHE
ΔE (V)	0.068
$i_p{}^c/i_p{}^a$	-2.8
Shift from E^o (V)	1.91

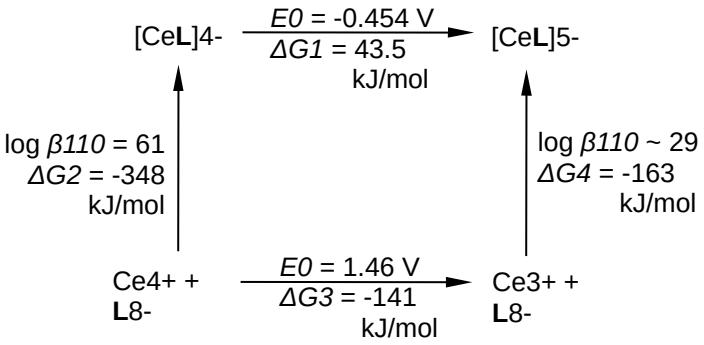

Figure 12. Thermodynamic cycle for the redox activity and **L** binding of cerium in KCl. The values for the complexation of Ce^{3+} were calculated from the equations $\Delta G_4 = -\Delta G_3 + \Delta G_2 + \Delta G_1$ and $\Delta G = -RTlnK$.

CONCLUSION.

In summary, the chemical and physical properties of a Ce^{4+} macrocyclic complex, Ce**L**K_4, were quantitatively measured. Solution-state thermodynamic measurements with the octadentate ligand **L** revealed a very strong preference for Ln^{4+} and An^{4+} ions, with a 29-order of magnitude difference in binding constants for Ce^{4+} relative to Pr^{3+}. These observations, and differences in bond distances from the solid-state crystal structures, can be rationalized by changes in charge and ionic radius. An exceptionally large, 7-order of magnitude difference in stability was also observed for Ce$\mathbf{L}^{4-}$ relative to Th$\mathbf{L}^{4-}$, which prompted an in-depth spectroscopic and theoretical analysis using Ce L_3- and $M_{5,4}$-edge XANES spectroscopies and configuration interaction calculations. These studies provided evidence for some covalent mixing between the Ce 4f and O 2p orbitals, and an increased contribution of the $4f^1\underline{L}$ LMCT configuration to the ground state. The magnitude of the LMCT was found to be similar to other formally Ce^{4+} compounds such as CeO_2 and $CeCl_6^{2-}$, but considerably less than that of cerocene, $(C_8H_8)_2Ce$.

A framework to rationalize these results can be developed using first-order perturbation theory (Figure 13), where increases in covalency are achieved by increasing overlap and decreasing the energy separation ($E_M^0 - E_L^0$) between the parent metal and ligand orbitals.[173-175] In this model, the 4f orbitals for

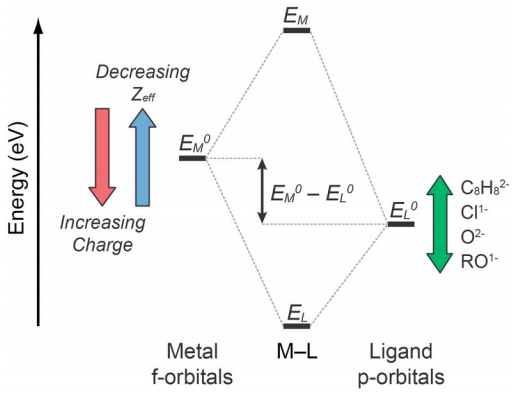

Figure 13. Qualitative molecular orbital diagram depicting the interaction between lanthanide 4f or actinide 5f orbitals and ligand 2p or 3p orbitals to form a metal–ligand bond. The energy gap ($E_M^0 - E_L^0$) can be decreased with softer (less electronegative) ligands. Lower energy f orbital potentials are found for higher oxidation states and metals later in the lanthanide or actinide series.

Ce^{4+} are lower in energy than the 4f orbitals for Pr^{3+} and the 5f orbitals for Th^{4+} because of greater effective nuclear charge.[2] Differences observed between Ce**L**$^{4-}$, $CeCl_6^{2-}$, CeO_2, and $(C_8H_8)_2Ce$ can thus be easily explained by differences in energy of the ligand 2p orbitals, which are higher for carbon and lower for more electronegative chloride and oxygen-based ligands. It is important to note that the energetic stabilization gained due to 4f covalency is proportional to the overlap between 4f and ligand-based orbitals.[173,175] Hence, because the radial extension of the 4f orbitals is very small,[176-179] increasing 4f covalency by decreasing the energy separation of the metal and ligand orbitals may act to weaken the bond overall by decreasing the amount of ionic character in the ground state.

This work also illustrates that thermodynamic, spectroscopic, and theoretical studies of tetravalent cerium molecules is a fruitful area for research. Configuration interaction calculations on free ions allow for interpretation of the $M_{5,4}$-edge spectra. New improvements in multiplet theory, together and experimental techniques that increase spectral resolution, will be valuable for future efforts to assign transitions in the L_3 and $M_{5,4}$-edges.[21-22] From the ligand's perspective, additional spectroscopic studies at the carbon, nitrogen, and oxygen K-edges can also provide a direct probe of bonding with both the 4f and 5d orbitals. Given the wide range of ligands that can stabilize tetravalent cerium in solution and the solid state, this is a unique opportunity to develop a deeper understanding of how subtle tuning of the electronic structure could lead to desirable physical properties or impact the outcome of chemical processes.

Supporting Information. Ce L_3-edge XANES data as well as the crystallographic information file for Ce**L**K_4. This material is available free of charge at http://pubs.acs.org.

ACKNOWLEDGEMENTS.

The authors would like to thank Dr. Michael Nippe for his invaluable help with electrochemical experiments. Booth, Lukens, Minasian, Olive, and Raymond were supported at LBNL by the Director, Office of Science, Office of Basic Energy Sciences, Division of Chemical Sciences, Geosciences, and Biosciences, Heavy Element Chemistry Program of the U.S. DOE under contract DE-AC02-05CH11231. Kozimor and Stieber were supported at LANL by the Director, Office of Science, Office of Basic Energy Sciences, Division of Chemical Sciences, Geosciences, and Biosciences, Heavy Element Chemistry Program of the U.S. DOE. LANL is operated by Los Alamos National Security, LLC, for the National Nuclear Security Administration of U.S. DOE under contract DE-AC52-06NA25396. Portions of this work were supported at the University of California, Berkeley by a DOE Integrated University Program Fellowship (Altman), at LANL by a Glenn T. Seaborg Institute Postdoctoral Fellowship (Stieber), and at the California State Polytechnic University, Pomona by the College of Science (Stieber). Research described in this paper was also performed at the Canadian Light Source, which is supported by the Canada Foundation for Innovation, Natural Sciences and Engineering Research Council of Canada, the University of Saskatchewan, the Government of Saskatchewan, Western Economic Diversification Canada, the National Research Council Canada, and the Canadian Institutes of Health Research. Tyliszczak and the ALS were supported at LBNL by the Director, Office of Science, Office of Basic Energy Sciences, of the U.S. DOE under contract DE-AC02-05CH11231. Research at Beamline 11.0.2 at the ALS was supported at LBNL by the Director, Office of Science, Office of Basic Energy Sciences, Division of Chemical Sciences, Geosciences, and Biosciences Condensed Phase and Interfacial Molecular Sciences Program of the U.S. DOE under contract DE-AC02-05CH11231. Use of the Stanford Synchrotron Radiation Lightsource, SLAC National Accelerator Laboratory, is supported by the U.S. Department of Energy, Office of Science, Office of Basic Energy Sciences under Contract No. DE-AC02-76SF00515.

References

(1) Cotton, F. A.; Wilkinson, G. *Advanced Inorganic Chemistry*; Wiley: New York, 1988.

(2) Martin, W. C.; Zalubas, R.; Hagan, L. *Atomic Energy Levels – The Rare Earth Elements*, NSRDS-NBS 60; U.S. Department of Commerce: Washington, DC, 1978.

(3) Kaatz, T.; Marcovich, M. *Acta Cryst.* **1966**, *21*, 1011.

(4) Penneman, R. A.; Rosenzweig, A. *Inorg. Chem.* **1969**, *8*, 627-630.

(5) Ryan, R. R.; Larson, A. C.; Kruse, F. H. *Inorg. Chem.* **1969**, *8*, 33-36.

(6) Meyer, G. *Prog. Solid State Chem.* **1982**, *14*, 141-219.

(7) Bianconi, A.; Marcelli, A.; Dexpert, H.; Karnatak, R.; Kotani, A.; Jo, T.; Petiau, J. *Phys. Rev. B* **1987**, *35*, 806-812.

(8) Bianconi, A.; Marcelli, A.; Tomellini, M.; Davoli, I. *J. Magn. Magn. Mater.* **1985**, *47-8*, 209-211.

(9) Nair, V.; Balagopal, L.; Rajan, R.; Mathew, J. *Acc. Chem. Res.* **2004**, *37*, 21-30.

(10) Nair, V.; Deepthi, A. *Chem. Rev.* **2007**, *107*, 1862-1891.

(11) Cross, J. N.; Duncan, P. M.; Villa, E. M.; Polinski, M. J.; Babo, J.-M.; Alekseev, E. V.; Booth, C. H.; Albrecht-Schmitt, T. E. *J. Am. Chem. Soc.* **2013**, *135*, 2769-2775.

(12) Kotani, A.; Ogasawara, H. *J. Electron. Spectrosc. Relat. Phenom.* **1992**, *60*, 257-299.

(13) Dallera, C.; Marcon, M.; Ghiringhelli, G.; Tagliaferri, A.; Brookes, N. B.; Olcese, G.; Palenzona, A.; Braicovich, L. *Solid State Commun.* **2002**, *121*, 635-640.

(14) Bianconi, A.; Campagna, M.; Stizza, S. *Phys. Rev. B* **1982**, *25*, 2477-2482.

(15) Bianconi, A.; Marcelli, A.; Davoli, I.; Stizza, S.; Campagna, M. *Solid State Commun.* **1984**, *49*, 409-415.

(16) Parks, R. D.; Raaen, S.; Denboer, M. L.; Murgai, V.; Mihalisin, T. *Phys. Rev. B* **1983**, *28*, 3556-3558.

(17) Dexpert, H.; Karnatak, R. C.; Esteva, J. M.; Connerade, J. P.; Gasgnier, M.; Caro, P. E.; Albert, L. *Phys. Rev. B* **1987**, *36*, 1750-1753.

(18) Kaindl, G.; Schmiester, G.; Sampathkumaran, E. V.; Wachter, P. *Phys. Rev. B* **1988**, *38*, 10174-10177.

(19) Gasgnier, M.; Schiffmacher, G.; Albert, L.; Caro, P. E.; Dexpert, H.; Esteva, J. M.; Blancard, C.; Karnatak, R. C. *J. Less-Common Met.* **1989**, *156*, 59-73.

(20) Le Fevre, P.; Magnan, H.; Chandesris, D.; Vogel, J.; Formoso, V.; Comin, F. *Phys. Rev. B* **1998**, *58*, 1080-1083.

(21) Kvashnina, K. O.; Butorin, S. M.; Glatzel, P. *J. Anal. At. Spectrom.* **2011**, *26*, 1265-1272.

(22) Kotani, A.; Kvashnina, K. O.; Butorin, S. M.; Glatzel, P. *Eur. Phys. J. B* **2012**, *85*, 257.

(23) Fuggle, J. C.; Hillebrecht, F. U.; Esteva, J. M.; Karnatak, R. C.; Gunnarsson, O.; Schonhammer, K. *Phys. Rev. B* **1983**, *27*, 4637-4643.

(24) Kaindl, G.; Kalkowski, G.; Brewer, W. D.; Perscheid, B.; Holtzberg, F. *J. Appl. Phys.* **1984**, *55*, 1910-1915.

(25) Thole, B. T.; Vanderlaan, G.; Fuggle, J. C.; Sawatzky, G. A.; Karnatak, R. C.; Esteva, J. M. *Phys. Rev. B* **1985**, *32*, 5107-5118.

(26) Jo, T.; Kotani, A. *Phys. Rev. B* **1988**, *38*, 830-833.

(27) Manoubi, T.; Colliex, C.; Rez, P. *J. Electron. Spectrosc. Relat. Phenom.* **1990**, *50*, 1-18.

(28) Grandjean, F.; Waddill, G. D.; Cummins, T. R.; Moore, D. P.; Long, G. J.; Buschow, K. H. J. *Solid State Commun.* **1998**, *108*, 593-597.

(29) Le Fevre, P.; Magnan, H.; Vogel, J.; Formoso, V.; Hricovini, K.; Chandesris, D. *J. Synchrotron Rad.* **1999**, *6*, 290-292.

(30) Dong, C. L.; Augustsson, A.; Chen, C. L.; Chang, C. L.; Chen, Y. Y.; Guo, J. H. *J. Electron. Spectrosc. Relat. Phenom.* **2005**, *144*, 581-584.

(31) Wu, Z. Y.; Jollet, F.; Gota, S.; Thromat, N.; Gautier-Soyer, M.; Petit, T. *J. Phys. Condens. Matter* **1999**, *11*, 7185-7194.

(32) Altman, A. B.; Pacold, J. I.; Wang, J.; Lukens, W. W.; Minasian, S. G. *Dalton Trans.* **2016**, accepted.

(33) Wuilloud, E.; Delley, B.; Schneider, W. D.; Baer, Y. *Phys. Rev. Lett.* **1984**, *53*, 202-205.

(34) Kotani, A.; Jo, T.; Parlebas, J. C. *Adv. Phys.* **1988**, *37*, 37-85.

(35) Sham, T. K.; Gordon, R. A.; Heald, S. M. *Phys. Rev. B* **2005**, *72*, 035113.

(36) Kotani, A. *Mod. Phys. Lett. B* **2013**, *27*, 1330012.

(37) Strange, P.; Svane, A.; Temmerman, W. M.; Szotek, Z.; Winter, H. *Nature* **1999**, *399*, 756-758.

(38) Skorodumova, N. V.; Ahuja, R.; Simak, S. I.; Abrikosov, I. A.; Johansson, B.; Lundqvist, B. I. *Phys. Rev. B* **2001**, *64*, 115108.

(39) Petit, L.; Svane, A.; Szotek, Z.; Temmerman, W. M. *Phys. Rev. B* **2005**, *72*, 205118.

(40) Hay, P. J.; Martin, R. L.; Uddin, J.; Scuseria, G. E. *J. Chem. Phys.* **2006**, *125*, 034712.

(41) Andersson, D. A.; Simak, S. I.; Johansson, B.; Abrikosov, I. A.; Skorodumova, N. V. *Phys. Rev. B* **2007**, *75*, 035109.

(42) Da Silva, J. L. F.; Ganduglia-Pirovano, M. V.; Sauer, J.; Bayer, V.; Kresse, G. *Phys. Rev. B* **2007**, *75*, 045121.

(43) Loschen, C.; Carrasco, J.; Neyman, K. M.; Illas, F. *Phys. Rev. B* **2007**, *75*, 035115.

(44) Jiang, H.; Gomez-Abal, R. I.; Rinke, P.; Scheffler, M. *Phys. Rev. Lett.* **2009**, *102*, 126403.

(45) Kullgren, J.; Castleton, C. W. M.; Muller, C.; Ramo, D. M.; Hermansson, K. *J. Chem. Phys.* **2010**, *132*, 054110.

(46) Gillen, R.; Clark, S. J.; Robertson, J. *Phys. Rev. B* **2013**, *87*, 125116.

(47) Anderson, P. W. *Phys. Rev.* **1961**, *124*, 41-53.

(48) Chen, Y. Y.; Huang, P. H.; Booth, C. H.; Lawrence, J. M. *Physica B* **2006**, *378-80*, 778-779.

(49) Fanelli, V. R.; Lawrence, J. M.; Goremychkin, E. A.; Osborn, R.; Bauer, E. D.; McClellan, K. J.; Thompson, J. D.; Booth, C. H.; Christianson, A. D.; Riseborough, P. S. *J. Phys. Condens. Matter* **2014**, *26*, 225602.

(50) Booth, C. H.; Han, S. W.; Skanthakumar, S.; Sarrao, J. L. *Physica B* **2004**, *354*, 313-319.

(51) Daniel, M.; Han, S. W.; Booth, C. H.; Cornelius, A. L.; Pagliuso, P. G.; Sarrao, J. L.; Thompson, J. D. *Phys. Rev. B* **2005**, *71*, 054417.

(52) Booth, C. H.; Bauer, E. D.; Bianchi, A. D.; Ronning, F.; Thompson, J. D.; Sarrao, J. L.; Cho, J. Y.; Chan, J. Y.; Capan, C.; Fisk, Z. *Phys. Rev. B* **2009**, *79*, 144519.

(53) Booth, C. H.; Durakiewicz, T.; Capan, C.; Hurt, D.; Bianchi, A. D.; Joyce, J. J.; Fisk, Z. *Phys. Rev. B* **2011**, *83*, 235117.

(54) Petrovic, C.; Pagliuso, P. G.; Hundley, M. F.; Movshovich, R.; Sarrao, J. L.; Thompson, J. D.; Fisk, Z.; Monthoux, P. *J. Phys. Condens. Matter* **2001**, *13*, L337-L342.

(55) Piro, N. A.; Robinson, J. R.; Walsh, P. J.; Schelter, E. J. *Coord. Chem. Rev.* **2014**, *260*, 21-36.

(56) Cassani, M. C.; Gun'ko, Y. K.; Hitchcock, P. B.; Hulkes, A. G.; Khvostov, A. V.; Lappert, M. F.; Protchenko, A. V. *J. Organomet. Chem.* **2002**, *647*, 71-83.

(57) Loeble, M. W. *et al. J. Am. Chem. Soc.* **2015**, *137*, 2506-2523.

(58) Bradley, D. C.; Chatterjee, A. K.; Wardlaw, W. *J. Chem. Soc.* **1956**, 2260-2264.

(59) Bradley, D. C.; Chatterjee, A. K.; Wardlaw, W. *J. Chem. Soc.* **1956**, 3469-3472.

(60) Gulino, A.; Casarin, M.; Conticello, V. P.; Gaudiello, J. G.; Mauermann, H.; Fragala, I.; Marks, T. J. *Organometallics* **1988**, *7*, 2360-2364.

(61) Evans, W. J.; Deming, T. J.; Olofson, J. M.; Ziller, J. W. *Inorg. Chem.* **1989**, *28*, 4027-4034.

(62) Evans, W. J.; Deming, T. J.; Ziller, J. W. *Organometallics* **1989**, *8*, 1581-1583.

(63) Sen, A.; Stecher, H. A.; Rheingold, A. L. *Inorg. Chem.* **1992**, *31*, 473-479.

(64) Gun'ko, Y. K.; Reilly, R.; Edelmann, F. T.; Schmidt, H. G. *Angew. Chem. Int. Ed.* **2001**, *40*, 1279-1281.

(65) Williams, U. J.; Schneider, D.; Dorfner, W. L.; Maichle-Moessmer, C.; Carroll, P. J.; Anwander, R.; Schelter, E. J. *Dalton Trans.* **2014**, *43*, 16197-16206.

(66) Williams, U. J.; Carroll, P. J.; Schelter, E. J. *Inorg. Chem.* **2014**, *53*, 6338-6345.

(67) Williams, U. J.; Robinson, J. R.; Lewis, A. J.; Carroll, P. J.; Walsh, P. J.; Schelter, E. J. *Inorg. Chem.* **2014**, *53*, 27-29.

(68) Behrsing, T.; Bond, A. M.; Deacon, G. B.; Forsyth, C. M.; Forsyth, M.; Kamble, K. J.; Skelton, B. W.; White, A. H. *Inorg. Chim. Acta* **2003**, *352*, 229-237.

(69) Gottfriedsen, J.; Hagner, R.; Spoida, M.; Suchorski, Y. *Eur. J. Inorg. Chem.* **2007**, 2288-2295.

(70) Droese, P.; Crozier, A. R.; Lashkari, S.; Gottfriedsen, J.; Blaurock, S.; Hrib, C. G.; Maichle-Moessmer, C.; Schaedle, C.; Anwander, R.; Edelmann, F. T. *J. Am. Chem. Soc.* **2010**, *132*, 14046-14047.

(71) Noh, W.; Girolami, G. S. *Polyhedron* **2007**, *26*, 3865-3870.

(72) Ashley, A.; Balazs, G.; Cowley, A.; Green, J.; Booth, C. H.; O'Hare, D. *Chem. Commun.* **2007**, 1515-1517.

(73) Eisenstein, O.; Hitchcock, P. B.; Hulkes, A. G.; Lappert, M. F.; Maron, L. *Chem. Commun.* **2001**, 1560-1561.

(74) Hitchcock, P. B.; Hulkes, A. G.; Lappert, M. F. *Inorg. Chem.* **2004**, *43*, 1031-1038.

(75) Hitchcock, P. B.; Lappert, M. F.; Protchenko, A. V. *Chem. Commun.* **2006**, 3546-3548.

(76) Coles, M. P.; Hitchcock, P. B.; Khvostov, A. V.; Lappert, M. F.; Li, Z.; Protchenko, A. V. *Dalton Trans.* **2010**, *39*, 6780-6788.

(77) Crozier, A. R.; Bienfait, A. M.; Maichle-Moessmer, C.; Tornroos, K. W.; Anwander, R. *Chem. Commun.* **2013**, *49*, 87-89.

(78) Schneider, D.; Spallek, T.; Maichle-Moessmer, C.; Toernroos, K. W.; Anwander, R. *Chem. Commun.* **2014**, *50*, 14763-14766.

(79) Buchler, J. W.; Decian, A.; Fischer, J.; Kihnbotulinski, M.; Paulus, H.; Weiss, R. *J. Am. Chem. Soc.* **1986**, *108*, 3652-3659.

(80) Lachkar, M.; Decian, A.; Fischer, J.; Weiss, R. *New J. Chem.* **1988**, *12*, 729-731.

(81) Buchler, J. W.; Decian, A.; Fischer, J.; Hammerschmitt, P.; Loffler, J.; Scharbert, B.; Weiss, R. *Chem. Ber.* **1989**, *122*, 2219-2228.

(82) Ikeda, M.; Takeuchi, M.; Sugasaki, A.; Robertson, A.; Imada, T.; Shinkai, S. *Supramol. Chem.* **2000**, *12*, 321-345.

(83) Bian, Y. Z.; Jiang, J. Z.; Tao, Y.; Choi, M. T. M.; Li, R. J.; Ng, A. C. H.; Zhu, P. H.; Pan, N.; Sun, X.; Arnold, D. P.; Zhou, Z. Y.; Li, H. W.; Mak, T. C. W.; Ng, D. K. P. *J. Am. Chem. Soc.* **2003**, *125*, 12257-12267.

(84) Walter, M. D.; Fandos, R.; Andersen, R. A. *New J. Chem.* **2006**, *30*, 1065-1070.

(85) Williams, U. J.; Mahoney, B. D.; Lewis, A. J.; DeGregorio, P. T.; Carroll, P. J.; Schelter, E. J. *Inorg. Chem.* **2013**, *52*, 4142-4144.

(86) Werner, D.; Deacon, G. B.; Junk, P. C.; Anwander, R. *Chem. Eur. J.* **2014**, *20*, 4426-4438.

(87) Bogart, J. A.; Lewis, A. J.; Medling, S. A.; Piro, N. A.; Carroll, P. J.; Booth, C. H.; Schelter, E. J. *Inorg. Chem.* **2013**, *52*, 11600-11607.

(88) Mahoney, B. D.; Piro, N. A.; Carroll, P. J.; Schelter, E. J. *Inorg. Chem.* **2013**, *52*, 5970-5977.

(89) Dorfner, W. L.; Carroll, P. J.; Schelter, E. J. *Dalton Trans.* **2014**, *43*, 6300-6303.

(90) Lee, H. B.; Bogart, J. A.; Carroll, P. J.; Schelter, E. J. *Chem. Commun.* **2014**, *50*, 5361-5363.

(91) Kim, J. E.; Carroll, P. J.; Schelter, E. J. *Chem. Commun.* **2015**, *51*, 15047-15050.

(92) Kurras, E.; Krüger, C.; Private Communication to the Cambridge Structural Database, deposit number CCDC 256935, 2004.

(93) Mares, F.; Hodgson, K.; Streitwieser, A. *J. Organomet. Chem.* **1970**, *24*, C68-C70.

(94) Greco, A.; Cesca, S.; Bertolini, G. *J. Organomet. Chem.* **1976**, *113*, 321-330.

(95) Hazin, P. N.; Bruno, J. W.; Brittain, H. G. *Organometallics* **1987**, *6*, 913-918.

(96) Dolg, M.; Fulde, P.; Kuchle, W.; Neumann, C. S.; Stoll, H. *J. Chem. Phys.* **1991**, *94*, 3011-3017.

(97) Kaltsoyannis, N.; Bursten, B. E. *J. Organomet. Chem.* **1997**, *528*, 19-33.

(98) Booth, C. H.; Walter, M. D.; Daniel, M.; Lukens, W. W.; Andersen, R. A. *Phys. Rev. Lett.* **2005**, *95*, 267202.

(99) Walter, M. D.; Booth, C. H.; Lukens, W. W.; Andersen, R. A. *Organometallics* **2009**, *28*, 698-707.

(100) Kerridge, A.; Coates, R.; Kaltsoyannis, N. *J. Phys. Chem. A* **2009**, *113*, 2896-2905.

(101) Kerridge, A. *Dalton Trans.* **2013**, *42*, 16428-16436.

(102) Moossen, O.; Dolg, M. *Chem. Phys. Lett.* **2014**, *594*, 47-50.

(103) Le Roy, J. J.; Korobkov, I.; Kim, J. E.; Schelter, E. J.; Murugesu, M. *Dalton Trans.* **2014**, *43*, 2737-2740.

(104) Robinson, J. R.; Gordon, Z.; Booth, C. H.; Carroll, P. J.; Walsh, P. J.; Schelter, E. J. *J. Am. Chem. Soc.* **2013**, *135*, 19016-19024.

(105) Bogart, J. A.; Lewis, A. J.; Boreen, M. A.; Lee, H. B.; Medling, S. A.; Carroll, P. J.; Booth, C. H.; Schelter, E. J. *Inorg. Chem.* **2015**, *54*, 2830-2837.

(106) Bogart, J. A.; Lippincott, C. A.; Carroll, P. J.; Booth, C. H.; Schelter, E. J. *Chem. Eur. J.* **2015**, *21*, 17850-17859.

(107) Robinson, J. R.; Carroll, P. J.; Walsh, P. J.; Schelter, E. J. *Angew. Chem. Int. Ed.* **2012**, *51*, 10159-10163.

(108) Bogart, J. A.; Lewis, A. J.; Schelter, E. J. *Chem. Eur. J.* **2015**, *21*, 1743-1748.

(109) Levin, J. R.; Dorfner, W. L.; Carroll, P. J.; Schelter, E. J. *Chem. Sci.* **2015**, *6*, 6925-6934.

(110) Corbey, J. F.; Woen, D. H.; Palumbo, C. T.; Fieser, M. E.; Ziller, J. W.; Furche, F.; Evans, W. J. *Organometallics* **2015**, *34*, 3909-3921.

(111) Fieser, M. E.; MacDonald, M. R.; Krull, B. T.; Bates, J. E.; Ziller, J. W.; Furche, F.; Evans, W. J. *J. Am. Chem. Soc.* **2015**, *137*, 369-382.

(112) MacDonald, M. R.; Bates, J. E.; Fieser, M. E.; Ziller, J. W.; Furche, F.; Evans, W. J. *J. Am. Chem. Soc.* **2012**, *134*, 8420-8423.

(113) MacDonald, M. R.; Bates, J. E.; Ziller, J. W.; Furche, F.; Evans, W. J. *J. Am. Chem. Soc.* **2013**, *135*, 9857-9868.

(114) MacDonald, M. R.; Fieser, M. E.; Bates, J. E.; Ziller, J. W.; Furche, F.; Evans, W. J. *J. Am. Chem. Soc.* **2013**, *135*, 13310-13313.

(115) La Pierre, H. S.; Scheurer, A.; Heinemann, F. W.; Hieringer, W.; Meyer, K. *Angew. Chem. Int. Ed.* **2014**, *53*, 7158-7162.

(116) Pham, T. A.; Xu, J.; Raymond, K. N. *J. Am. Chem. Soc.* **2014**, *136*, 9106-9115.

(117) Durbin, P. W.; Kullgren, B.; Xu, J.; Raymond, K. N. *Radiat. Prot. Dosim.* **1998**, *79*, 433-443.

(118) Gorden, A. E. V.; Xu, J. D.; Raymond, K. N.; Durbin, P. *Chem. Rev.* **2003**, *103*, 4207-4282.

(119) Sturzbecher-Hoehne, M.; Clara Ng Pak, L.; D'Aleo, A.; Kullgren, B.; Prigent, A.-L.; Shuh, D. K.; Raymond, K. N.; Abergel, R. J. *Dalton Trans.* **2011**, *40*, 8340-8346.

(120) Diamond, R. M.; Street, K.; Seaborg, G. T. *J. Am. Chem. Soc.* **1954**, *76*, 1461-1469.

(121) Choppin, G. R. *J. Less-Common Met.* **1983**, *93*, 323-330.

(122) Xu, J. D.; Radkov, E.; Ziegler, M.; Raymond, K. N. *Inorg. Chem.* **2000**, *39*, 4156-4164.

(123) Raymond, K. N.; Szigethy, G. *MRS Online Proceedings Library Archive* **2008**, *1104*, NN04-01.

(124) Gorden, A. E. V.; Xu, J.; Szigethy, G.; Oliver, A.; Shuh, D. K.; Raymond, K. N. *J. Am. Chem. Soc.* **2007**, *129*, 6674-6675.

(125) Szigethy, G.; Xu, J.; Gorden, A. E. V.; Teat, S. J.; Shuh, D. K.; Raymond, K. N. *Eur. J. Inorg. Chem.* **2008**, 2143-2147.

(126) Mikheev, N. B.; Kulyukhin, S. A.; Melikhov, I. V. *Radiochemistry*, *49*, 449-463.

(127) Sturzbecher-Hoehne, M.; Choi, T. A.; Abergel, R. J. *Inorg. Chem.* **2015**, *54*, 3462-3468.

(128) Shannon, R. D. *Acta Crystallogr. A* **1976**, *32*, 751-767.

(129) Morss, L. R. In *Handbook on the Physics and Chemistry of Rare Earths*; Gschneider, K. A., Eyring, L., Choppin, G. R., Lander, G. H., Eds.; Elsevier Science: Amsterdam, 1994; Vol. 18, p 239-291.

(130) Bruker Analytical X-ray Systems, I., SADABS: Bruker Nonius Area Detector Scaling and Absorption, Madison, WI

(131) Sheldrick, G. M. *Acta Crystallogr. A* **2008**, *64*, 112-122.

(132) Farrugia, L. *J. Appl. Crystallogr.* **1999**, *32*, 837-838.

(133) Bradley, J. A.; Yang, P.; Batista, E. R.; Boland, K. S.; Burns, C. J.; Clark, D. L.; Conradson, S. D.; Kozimor, S. A.; Martin, R. L.; Seidler, G. T.; Scott, B. L.; Shuh, D. K.; Tyliszczak, T.; Wilkerson, M. P.; Wolfsberg, L. E. *J. Am. Chem. Soc.* **2010**, *132*, 13914-13921.

(134) Magnuson, M.; Butorin, S. M.; Werme, L.; Nordgren, J.; Ivanov, K. E.; Guo, J. H.; Shuh, D. K. *Appl. Surf. Sci.* **2006**, *252*, 5615-5618.

(135) Minasian, S. G. *et al. J. Am. Chem. Soc.* **2013**, *135*, 1864-1871.

(136) Meihaus, K. R.; Minasian, S. G.; Lukens, W. W.; Kozimor, S. A.; Shuh, D. K.; Tyliszczak, T.; Long, J. R. *J. Am. Chem. Soc.* **2014**, *136*, 6056-6068.

(137) Kaznatcheev, K. V.; Karunakaran, C.; Lanke, U. D.; Urquhart, S. G.; Obst, M.; Hitchcock, A. P. *Nucl. Instrum. Methods Phys. Res. A* **2007**, *582*, 96-99.

(138) Bluhm, H. *et al. J. Electron. Spectrosc. Relat. Phenom.* **2006**, *150*, 86-104.

(139) Nilsson, H. J.; Tyliszczak, T.; Wilson, R. E.; Werme, L.; Shuh, D. K. *Anal. Bioanal. Chem.* **2005**, *383*, 41-47.

(140) Tyliszczak, T.; Warwick, T.; Kilcoyne, A. L. D.; Fakra, S.; Shuh, D. K.; Yoon, T. H.; Brown, G. E.; Andrews, S.; Chembrolu, V.; Strachan, J.; Acremann, Y. In *Synchrotron Radiation Instrumentation 2003, AIP Conference Proceedings* 2004; Vol. 705, p 1356-1359.

(141) Keski-Rahkonen, O.; Krause, M. O. *At. Data Nucl. Data Tables* **1974**, *14*, 139-146.

(142) Cowan, R. D. *Theory of Atomic Structure and Spectra*; University of California Press, 1981.

(143) de Groot, F. M. F.; Kotani, A. *Core Level Spectroscopy of Solids*; Taylor and Francis: New York, 2008.

(144) Gans, P.; O'Sullivan, B. *Talanta* **2000**, *51*, 33-37.

(145) Gans, P.; Sabatini, A.; Vacca, A. *Talanta* **1996**, *43*, 1739-1753.

(146) Gans, P.; Sabatini, A.; Vacca, A. *Ann. Chim. (Rome)* **1999**, *89*, 45-49.

(147) Smith, R. M.; Martell, A. E.; Motekaitis, R. J. *NIST Critically Selected Stability Constants of Metal Complexes Database*, NIST Standard Reference Database 46; NIST: Gaithersburg, MD, 2001.

(148) Suzuki, Y.; Nankawa, T.; Francis, A. J.; Ohnuki, T. *Radiochim. Acta* **2010**, *98*, 397-402.

(149) Alderighi, L.; Gans, P.; Ienco, A.; Peters, D.; Sabatini, A.; Vacca, A. *Coord. Chem. Rev.* **1999**, *184*, 311-318.

(150) Gonzalez-Mendoza, R.; Lopez-Gonzalez, H.; Rojas-Hernandez, A. *J. Mex. Chem. Soc.* **2010**, *54*, 51-58.

(151) Farrugia, L. *J. Appl. Crystallogr.* **1997**, *30*, 565.

(152) Deblonde, G. J. P.; Sturzbecher-Hoehne, M.; Abergel, R. J. *Inorg. Chem.* **2013**, *52*, 8805-8811.

(153) Doble, D. M. J.; Melchior, M.; O'Sullivan, B.; Siering, C.; Xu, J. D.; Pierre, V. C.; Raymond, K. N. *Inorg. Chem.* **2003**, *42*, 4930-4937.

(154) Karnatak, R. C. *J. Alloys Compd.* **1993**, *192*, 64-68.

(155) Kotani, A.; Kvashnina, K. O.; Butorin, S. M.; Glatzel, P. *J. Electron. Spectrosc. Relat. Phenom.* **2011**, *184*, 210-215.

(156) Hu, Z.; Kaindl, G.; Ogasawara, H.; Kotani, A.; Felner, I. *Chem. Phys. Lett.* **2000**, *325*, 241-250.

(157) Jo, T.; Kotani, A. *J. Phys. Soc. Jpn.* **1988**, *57*, 2288-2291.

(158) Minasian, S. G. *unpublished*.

(159) At this stage, efforts to obtain reproducible $M_{5,4}$-edge XANES spectra of $(C_8H_8)_2Ce$ have been thwarted by difficulties associated with highly X-ray photon sensitive material

(160) Stavitski, E.; de Groot, F. M. F. *Micron* **2010**, *41*, 687-694.

(161) de Groot, F. *Coord. Chem. Rev.* **2005**, *249*, 31-63.

(162) Kucheyev, S. O.; Clapsaddle, B. J.; Wang, Y. M.; van Buuren, T.; Hamza, A. V. *Phys. Rev. B* **2007**, *76*, 235420.

(163) Turner, S.; Lazar, S.; Freitag, B.; Egoavil, R.; Verbeeck, J.; Put, S.; Strauven, Y.; Van Tendeloo, G. *Nanoscale* **2011**, *3*, 3385-3390.

(164) Dolg, M.; Fulde, P.; Stoll, H.; Preuss, H.; Chang, A.; Pitzer, R. M. *Chem. Phys.* **1995**, *195*, 71-82.

(165) Konings, R. J. M.; Morss, L. R.; Fuger, J. In *The Chemistry of the Actinide and Transactinide Elements*; Morss, L. R., Edelstein, N. M., Fuger, J., Eds.; Springer Netherlands: Dordrecht, 2006, p 2113-2224.

(166) Sofen, S. R.; Cooper, S. R.; Raymond, K. N. *Inorg. Chem.* **1979**, *18*, 1611-1616.

(167) Haddad, S. F.; Raymond, K. N. *Inorg. Chim. Acta* **1986**, *122*, 111-118.

(168) Wester, D. W.; Palenik, G. J.; Palenik, R. C. *Inorg. Chem.* **1985**, *24*, 4435-4437.

(169) Bard, A. J.; Faulkner, L. R. *Electrochemical Methods: Fundamentals and Applications*; 2nd ed.; Wiley: New York, 2001.

(170) Wadsworth, E.; Duke, F. R.; Goetz, C. A. *Anal. Chem.* **1957**, *29*, 1824-1825.

(171) Brown, M. A.; Paulenova, A.; Gelis, A. V. *Inorg. Chem.* **2012**, *51*, 7741-7748.

(172) Morss, L. R.; Fuger, J. *J. Inorg. Nucl. Chem.* **1981**, *43*, 2059-2064.

(173) Minasian, S. G.; Kieth, J. M.; Batista, E. R.; Boland, K. S.; Christensen, C. N.; Clark, D. L.; Conradson, S. D.; Kozimor, S. A.; Martin, R. L.; Schwarz, D. E.; Shuh, D. K.; Wagner, G. L.; Wilkerson, M. P.; Wolfsberg, L. E.; Yang, P. *J. Am. Chem. Soc.* **2012**, *134*, 5586-5597.

(174) Kaltsoyannis, N. *Inorg. Chem.* **2013**, *52*, 3407-3413.

(175) Neidig, M. L.; Clark, D. L.; Martin, R. L. *Coord. Chem. Rev.* **2013**, *257*, 394-406.

(176) Crosswhite, H. M.; Crosswhite, H.; Carnall, W. T.; Paszek, A. P. *J. Chem. Phys.* **1980**, *72*, 5103-5117.

(177) Cundari, T. R.; Stevens, W. J. *J. Chem. Phys.* **1993**, *98*, 5555-5565.

(178) Vetere, V.; Maldivi, P.; Adamo, C. *J. Comput. Chem.* **2003**, *24*, 850-858.

(179) Atanasov, M.; Daul, C.; Gudel, H. U.; Wesolowski, T. A.; Zbiri, M. *Inorg. Chem.* **2005**, *44*, 2954-2963.

For Table of Contents Only

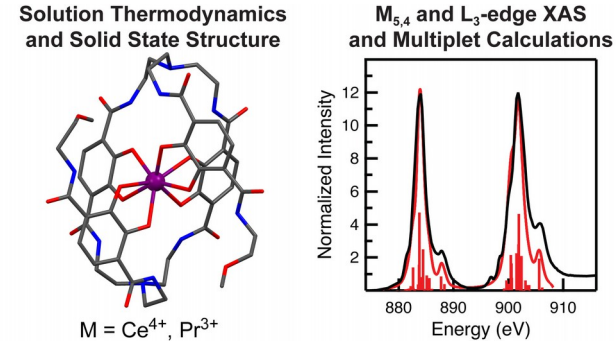

A complex of Ce^{4+} with a macrocyclic ligand was characterized by spectrophotometric titrations, electrochemistry, and X-ray diffraction studies, which demonstrated a remarkable affinity of the ligand towards Ce^{4+}, particularly relative to the analogous trivalent lanthanide and tetravalent actinide. L_3 and $M_{5,4}$-edge X-ray absorption near-edge structure spectroscopies and configuration interaction calculations were used to characterize 4f-orbital bonding in the complex.